UNIVERSITY OF SASKATCHEWAN

ABSORPTION OF SUNLIGHT BY ATMOSPHERIC SODIUM USING A FABRY-PEROT SPECTROMETER AND A SODIUM VAPOUR CELL

A

Thesis

submitted to

THE FACULTY OF GRADUATE STUDIES

in partial fulfilment of

the requirements for

THE DEGREE OF MASTER OF SCIENCE

in

THE DEPARTMENT OF PHYSICS

UNIVERSITY OF SASKATCHEWAN

by

Yee Pan Neo

Saskatoon, Saskatchewan

September, 1963

ACKNOWLEDGMENTS

The author wishes to express his sincere gratitude to Dr. G. G. Shepherd, who supervised the research reported in this thesis. Dr. Shepherd's patient guidance and constructive advice during the period of research have been most helpful.

The author also wishes to thank Dr. D. M. Hunten, who made available the sodium vapour cell and the temperature regulator for use in this experiment.

Thanks are due to the Canadian Commonwealth Scholarship and Fellowship Plan Committee for giving the author the opportunity to come to Canada and for providing the financial aid in the form of a Commonwealth Scholarship.

The use of the facilities provided by the Physics Department is gratefully acknowledged.

ABSTRACT

A low-resolution Fabry-Perot spectrometer was used in conjunction with a sodium vapour cell to observe the terrestrial absorption by sodium. By observing the variation of absorption with the solar elevation, the sodium abundance was determined. The abundances of sodium obtained were in the range between 16 X 10^9 and 20 X 10^9 atoms/cm^2 column. Recent dayglow results obtained by Blamont and Donahue (1961) have indicated that the sodium abundance in the daytime is three to four times higher than during twilight. The present results tend to support the dayglow observation by Blamont and Donahue (1961). However, previous work by Zwick and Shepherd (1961) and McNutt and Mack (1963) have both indicated no enhancement of sodium during the daytime as compared to twilight. The apparent contradiction between these sets of results has not yet been resolved.

As an additional result, the residual intensities at the bottom of the Fraunhofer D-lines were found to be 6.37 $\pm$ 0.19% and 5.41 $\pm$ 0.25% for the D_1 and D_2 lines respectively.

TABLE OF CONTENTS

Table of Contents--Continued

- - -

LIST OF TABLES

- - -

LIST OF FIGURES

List of Figures--Continued

- - -

LIST OF SYMBOLS

p_o: residual intensity at the bottom of the Fraunhofer D-lines, with no terrestrial absorption by sodium, expressed as a percentage of the continuum.

p_e: the effective residual intensity at the bottom of the Fraunhofer lines after terrestrial absorption, expressed as a percentage of the continuum.

τ_o: the optical thickness at the centre of the sodium D-lines.

τ_e: the effective optical thickness of the atmospheric sodium.

$I_S(\sigma)$: the solar intensity incident on the atmosphere.

$I_T(\sigma)$: solar intensity after transmissions through the sodium layer.

I_o: intensity at the bottom of the Fraunhofer D-lines with no absorption by sodium.

I_{TC}: spectrum of D-lines after transmission through the sodium cell before the Fabry-Perot etalon.

I_L: brightness of the calibration lamp.

L: luminosity of the Fabry-Perot spectrometer.

$k_T N_T$: optical thickness along the path of the solar beam.

$k_C N_C$: optical thickness of the sodium vapour cell.

List of Symbols--Continued

Y_{TM}, Y_{LM}: recorded signals of the sun and the lamp in the monitor channel.

Y_{TR}, Y_{LR}: recorded signals of the sun and the lamp in the cell channel.

Y'_{TM}, Y'_{LM}, Y'_{TR}, Y'_{LR}: areas under the corresponding line profiles.

$\bar{k}$: the effective absorption coefficient of the sodium D-lines.

α: the angle between the solar beam and the normal to the sodium layer at the point of intersection.

$\sec.\alpha$: the relative path length of the solar beam.

- - -

I. INTRODUCTION

The earth's upper atmosphere has attracted the attention of many research workers and considerable effort has been directed toward revealing the secrets that lie within it. Various measuring devices including the spectrometer and the photometer have been used in an attempt to study the behaviour of the atmospheric constituents. Although theoretical and experimental advancement has been made, many problems still remain unsolved and many experimental facts unexplained.

Among the various atmospheric processes studied, the emission of the sodium D-lines during twilight is a problem that has engaged the attention of many workers. This is probably due to the fact that sodium is one of the few atmospheric constituents that is amenable to a fairly complete theoretical and observational analysis. Chamberlain, Hunten, and Mack (1958) and Chamberlain (1961) have given a comprehensive treatment of the theoretical aspects of the problem.

One quantity of great interest to geophysicists is the

abundance of free sodium atoms (atoms/cm^2 column) present in the atmosphere during the day and during twilight. Bullock and Hunten (1961) have observed the seasonal variation of the twilight sodium in Saskatoon with a birefringent photometer. They have established that the abundance of free sodium atoms is usually between 4.7×10^9 and 1.0×10^9 atoms/cm^2 column and that it can be as large as 7.0×10^9 atoms/cm^2 column. According to measurements made during twilight by Blamont and Donahue (1958) and Donahue and Blamont (1960), the number of free sodium atoms can be as high as 30×10^9 atoms/cm^2 column. This disagreement is yet to be resolved and probably lies in the fact that the abundance of sodium might vary with the geographical situations.

Although the twilight sodium abundance has been fairly thoroughly measured (Bullock and Hunten, 1961; Zwick and Shepherd, 1962), the problem of the sodium dayglow is hardly touched upon. Until recently, the measurement of the sodium dayglow has not been attempted, mainly because of the difficulty in contending with the strong background of white light scattered in the troposphere. It was pointed out a long time ago by Bricard and Kastler (1944) that the sodium emission under the most favourable condition might not be weak compared to that scattered by the lower atmosphere in the same wavelength interval.

Thus far, only two attempts have been made at calculating the sodium dayglow intensity, one by Donahue (1956) and one by Brandt and Chamberlain (1958). As far as the experimental work is concerned, the only earlier observations providing evidence of the amount of sodium in the daytime are those of Scrimger and Hunten (1957) and Blamont and Donahue (1961). The first of these authors observed the effect of absorption by atmospheric sodium on the Fraunhofer lines during the course of the day. Using sunlight as the source, the light was directed into a sodium vapour cell with low number density and the scattered light was recorded by a photoelectric spectrometer. By observing the variation of absorption with solar elevation, the sodium abundance was then deduced. Since the radiation detected was at the bottom of the Fraunhofer lines, the residual intensities there were measured as a by-product. The latter authors observed the sodium dayglow in the scattered sunlight using a Zeeman-modulated resonance scattering cell. The cell was temperature controlled, with provision for observation of the light scattered at right angles to the incident beam. A magnetic field of 4000 gauss was used to shift the passband into the continuum and the difference between field-on and field-off readings was reckoned to be the D-line intensity. The measured day emission was reported to be three to four times

as large as those observed during twilight. However, the above method required an accurate knowledge of the solar profile in addition to the fact that no atmospheric lines other than sodium must be present within the region swept by the magnetic field; i.e., 300 mK (1 mK = 10^{-3} cm^{-1}). Recently, measurements were made by McNutt (1962) of terrestrial absorption of solar radiation using a high resolution Fabry-Perot spectrometer coupled to a grating spectrometer, and the results indicated the daytime sodium abundance to be the same as during twilight. Also, work by Zwick and Shepherd (1962) using a low-resolution scanning Fabry-Perot spectrometer in measuring the ratio and absolute brightness of the sodium D-lines in the twilight glow has indirectly indicated lack of sodium enhancement during the day.

The present thesis is devoted to the study of the daytime sodium in the light of the recent results obtained by Blamont and Donahue (1961). As mentioned earlier, their results indicated daytime sodium abundance to be three to four times higher than those during twilight. Consequently, it was considered worthwhile to repeat the experiment of Scrimger and Hunten (1957) in the hope of obtaining more evidence as regards the sodium abundance during the day. However, the experimental arrangement differed slightly. In

Scrimger and Hunten's experiment, the sodium resonance cell was used to scatter the incident light into the photoelectric spectrometer, and each measurement required a period of about 20 minutes. A number of such measurements must be obtained during the day to determine the sodium abundance. In the present experiment, however, a low-resolution Fabry-Perot spectrometer was employed, and light was passed through the spectrometer before being scattered by the sodium cell. Moreover, the present instrument consisted of two channels, thus enabling each measurement to be made in two minutes, giving more data points per run. In this experiment, the residual intensities at the bottom of the Fraunhofer lines will be measured as a by-product.

Chapter 2 describes the experimental aspects and the observational techniques. The theory of the sodium absorption is presented in Chapter 3. The results obtained and the method of analysis are contained in Chapter 4. A summary and suggestions for further work are found in Chapter 5.

2. EXPERIMENTAL

2.1 Introduction

As already mentioned, the abundance of free sodium atoms in the upper atmosphere is a quantity of importance to the geophysicists. This quantity can be deduced from absolute brightness measurements of the sodium D-lines in twilight. However, two major difficulties are encountered when using this procedure. The first is due to self-absorption, which is caused by the sodium itself and which has the tendency to reduce the apparent brightness. Hence, correction must be allowed for this effect. Secondly, there is the uncertainty as regards the incident solar flux, which is not known accurately. This uncertainty arises mostly in the measurements of the residual intensities at the bottom of the Fraunhofer lines.

Several attempts to determine the residual intensities at the bottom of the Fraunhofer lines have been made by solar physicists such as Allen (1939), Priester (1933), Shane (1941), and Waddel (1962). Two attempts to verify these values were made by Scrimger and Hunten (1955, 1957). The

latter experiment made use of a sodium vapour cell, which scattered the incident sunlight into a photoelectric spectrometer. The spectrometer resolved the two sodium D-lines and eliminated the effect of the parasitic scattered spectrum. The principal result obtained was the sodium abundance in the daytime, and the residual intensities were measured as a by-product.

In the present experiment, a Fabry-Perot spectrometer was used in conjunction with a sodium vapour cell. A block diagram of the whole assembled apparatus is shown in Fig. 2.1. The incident sunlight was first directed into a photoelectric Fabry-Perot spectrometer using an interference filter as a low resolution monochromator. This effectively isolated a single etalon passband. The light was then scattered by the sodium vapour cell and recorded by a photomultiplier. The recorded signal was that of the sodium D-lines denoted by d_s in Fig. 2.2a. (The white light continuum is stray light.) This is a measure of the amount of sodium remaining at the bottom of the Fraunhofer lines after absorption in the solar and terrestrial atmosphere. A beam-splitter was placed between the Fabry-Perot etalon and the resonance cell. The beam-splitter, which consisted of a glass plate, was mounted at an angle so as to reflect a small portion of the transmitted light into a photomultiplier in

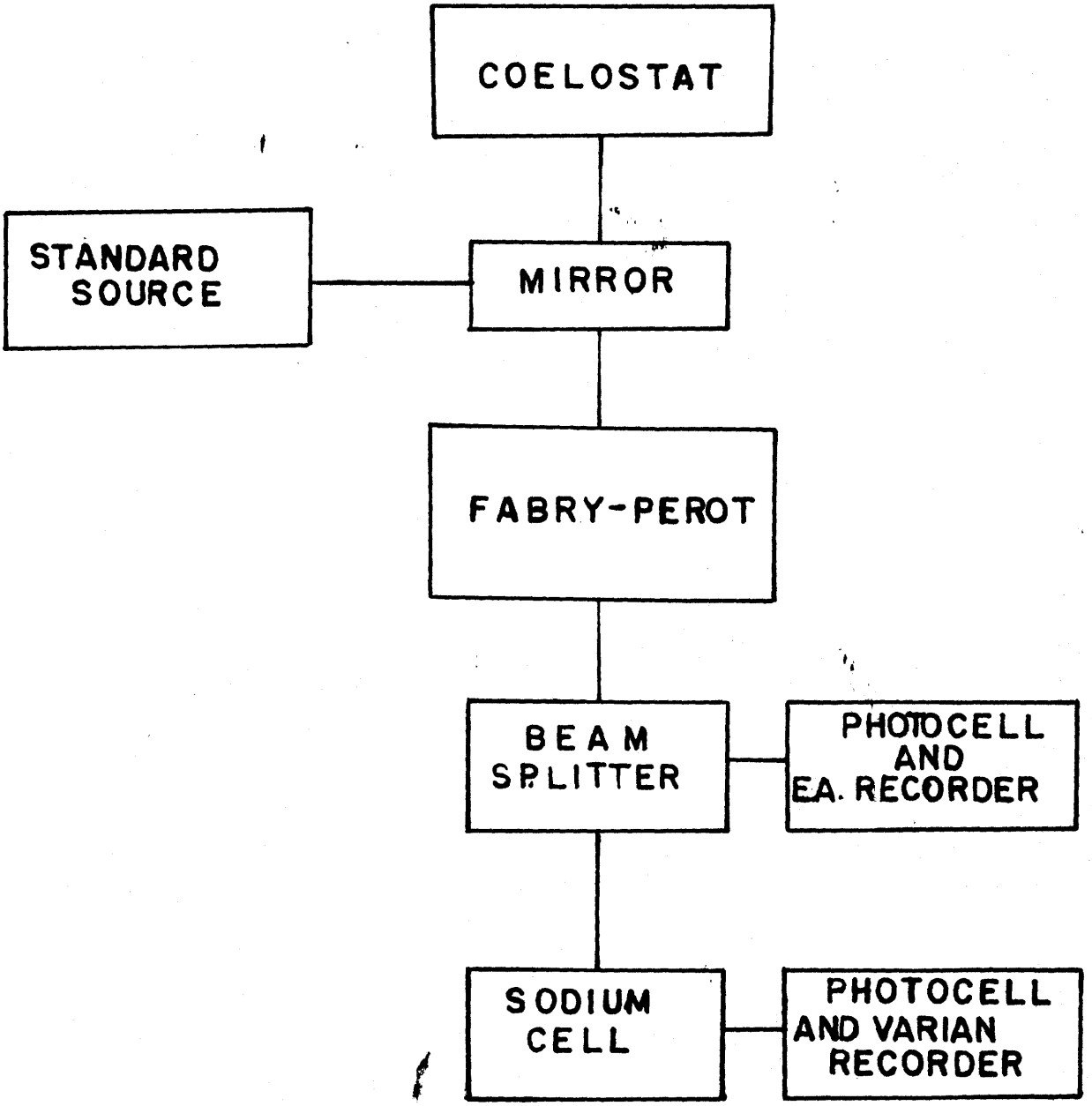

Fig.2.1 Block diagram of the assembled apparatus

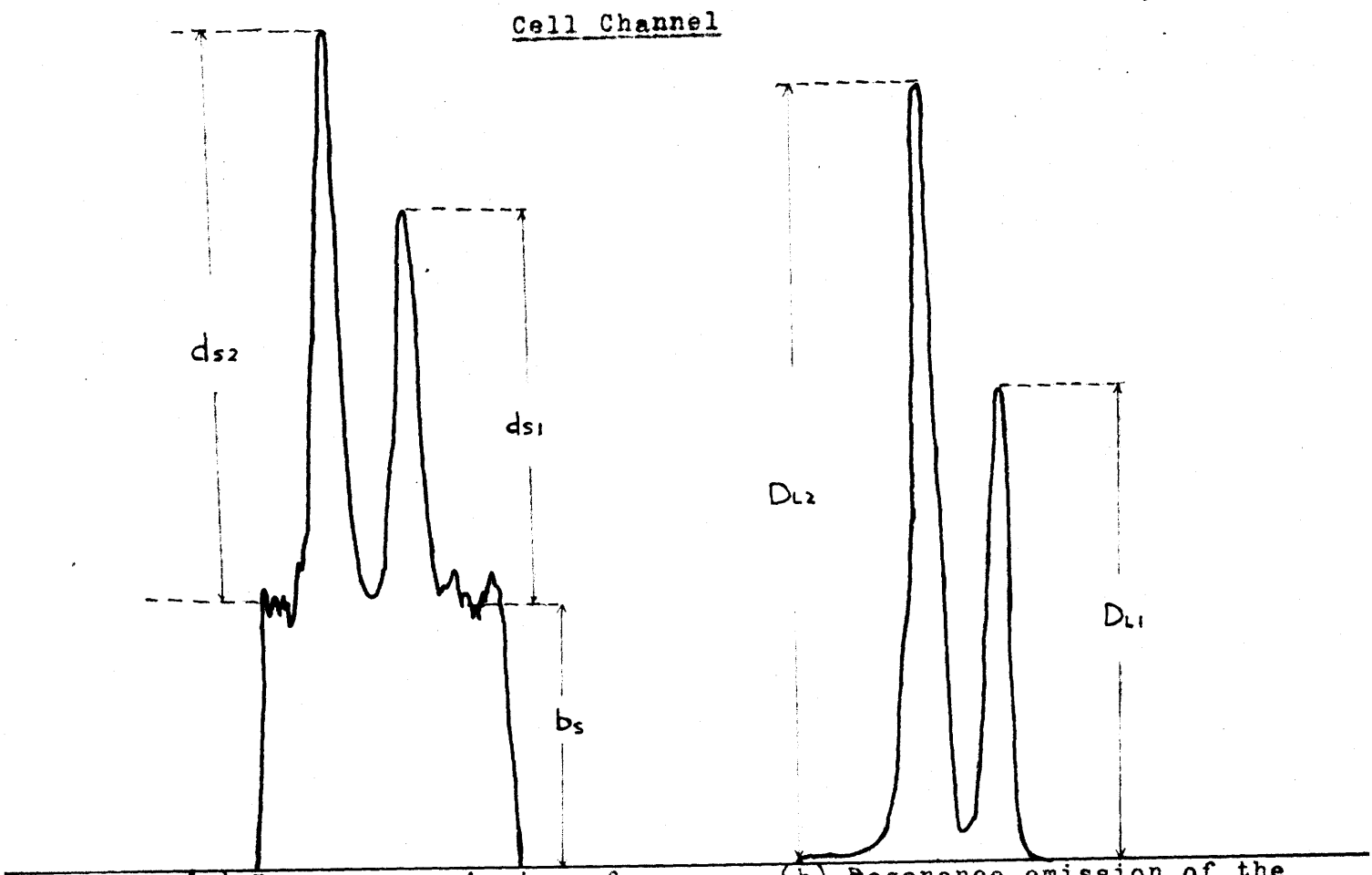

Fig.2.2(a) Resonance emission of the D-lines using sunlight

(b) Resonance emission of the D-lines using calibration lamp

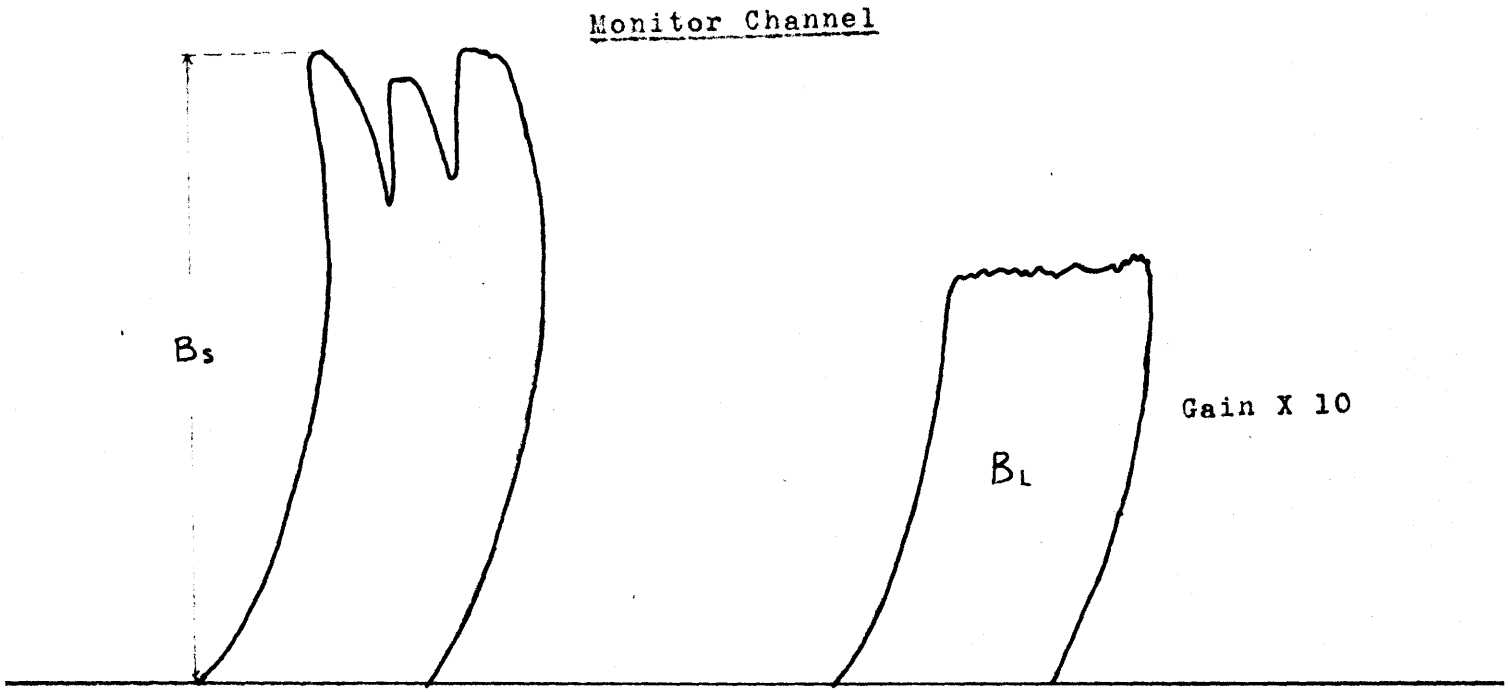

(c) Spectrum of scattered sunlight

(d) Continuum of scattered light from the calibration lamp

another channel. This recorded the spectrum of the background level B_s (Fig. 2.2c), indicating the continuum intensity on both sides of the D-lines. The Fraunhofer absorption lines can be seen; but because of the low resolution, they give no indication of the true depth of the absorption lines. The ratio of these two signals yields the intensity remaining at the bottom of D-lines after absorption by the sodium layer, expressed as a fraction of the continuum. This will be denoted by p_1 and p_2 for the D_1 and D_2 lines respectively. To calculate this, the relative sensitivities of the two channels must be known. To calibrate this, a white light tungsten source was used, producing two spectra, one in each channel as shown in Fig. 2.2b and d. The spectrum b was recorded by the sodium cell channel, and the spectrum d gave the amount of white light transmitted by the etalon of the Fabry-Perot spectrometer.

In this chapter, the Fabry-Perot spectrometer, the resonance cell, and the calibration lamp unit will be described. A general description of the experimental arrangement as well as the observational procedure will also be presented.

2.2 The Fabry-Perot Spectrometer

The use of the Fabry-Perot spectrometer in conjunction with photographic spectrographs for high resolution studies

is well known. This apparatus, invented in 1896, has been employed chiefly in the investigation of hyperfine structures. For a long time the apparatus was very little developed, and its use was limited mainly to this kind of investigation.

In recent years, however, it was realized that its use could be extended beyond the photographic method and over a large range of resolution. Considerable progress both theoretical as well as practical has been achieved. The instrument was recently developed into a scanning photoelectric spectrometer, mainly by Chabbal (1953, 1958a, b), and is currently being extensively employed in the studies of the airglow and the aurora. The reason that this instrument is most suited to such observations is that it possesses a high light gathering power, much higher than that of a grating spectrometer operating at the same resolution (P. Jacquinot, 1954). That is, if the light gathering power is denoted by G, the area of the selective element by A, the solid angle it will receive by Ω, and the transmission of the instrument by T, then $G = A\Omega T$. Furthermore, if R is the resolving power of the instrument, GR is a constant for any spectrometer; but this constant has a much higher value for the Fabry-Perot spectrometer than for a grating spectrometer if both have the same area A. Shepherd (1960), Zwick and

Shepherd (1962), Nilson and Shepherd (1960), Turgeon and Shepherd (1961), and Cogger (1962) have thoroughly demonstrated the capability of the Fabry-Perot spectrometer in the observations of the airglow and the aurora.

The elementary theory of the instrument is well known and is treated in most optics textbook. Chabbal (1953) first worked out the detailed theory of the photoelectric Fabry-Perot spectrometer, and reviews of this paper have been given by P. Jacquinot (1960) and Nilson (1960). Only a brief description dealing with the essential features of the spectrometer will be given here.

In general, the Fabry-Perot spectrometer is an ensemble which includes, in series, the source, a monochromator, the Fabry-Perot etalon, and an isolating diaphragm followed by a detector. The Fabry-Perot etalon is the most important component of the spectrometer and consists of a pair of transparent quartz plates having partially reflecting inner surfaces. In the ideal case, the plates are perfectly flat and parallel. When a light beam (of a given wavelength) is incident upon the two parallel plates, it is divided by multiple transmissions and reflections into an infinity of rays reflected and transmitted parallel to each other. The transmitted rays, the ones used in general, recombine at infinity and interfere. Between two successive transmitted

rays, there is an optical path difference. If this optical path difference is an integral number of wavelengths, the transmitted rays will interfere constructively and the incident energy is transmitted. Since the path difference depends on the angle of incidence, the transmitted rays form a system of rings which is centered on the optical axis of the instrument. Hence if a lens is placed so that the diaphragm is at its focal plane, the Fabry-Perot passband can be isolated. If the path difference is not an integral number of wavelengths, multiple rays interfere destructively, and the incident energy is reflected back to the source.

Thus for a given value of the optical path difference, the Fabry-Perot device acts as a wavelength filter; and if the optical path between the plates is varied, the transmitting passbands can be made to sweep across a wavelength interval. This means that the etalon can be set either to transmit a desired wavelength or can be used to traverse a spectral region. In either case, the optical separation between the plates must be made controllable. Two methods are widely in use. One is by varying the refractive index of the gas surrounding the plates (Nilson, 1960 and Cogger, 1962). The other is to move mechanically one of the plates without destroying the parallelism. The present instrument is the one designed by Zwick and Shepherd (1962), who adopted

the method of mechanical scanning. At the low order (about 300) in which the instrument is operating, mechanical scanning is advantageous since a large scanning range is desired (Shepherd, 1960). The passband separation in this case is about 20 Å, and an interference filter with a passband half-width of 15 Å is used as a monochromator to isolate a single passband. The filter is tilted at an angle, and the angle is changed with time so that its scan is synchronized with that of the Fabry-Perot etalon. This enables a constant transmission of light to be obtained. In this way, the detector is made to receive energy only from a single passband (having a half-width of about 1.5 Å) of the Fabry-Perot etalon.

2.3 The Sodium Resonance Cell

The sodium resonance cell used in this experiment was constructed and described by Scrimger (1956). For completeness, a brief description only will be presented here.

In short, a resonance cell is a glass vessel containing an unexcited gas or vapour which can absorb a beam of radiation from an external source (an "exciting" source) and which, as a result of this optical excitation, emits resonance radiation in all directions. As a definition, resonance radiation may be said to be the light emitted by atoms originally in the ground state which, after absorbing light of a certain frequency, subsequently re-emit light of the same frequency. In

terms of the quantum concept, resonance radiation will occur when an atom is excited to a higher quantum state from the ground state by absorption of one quantum of light and then return to the same state by the emission of one quantum of radiation. As already mentioned, in this process, light of the same frequency as that absorbed will be emitted. This differs from the well-known process of fluorescence in the fact that in fluorescence the frequency of radiation emitted is different from that which is absorbed.

The resonance radiation of sodium has been thoroughly investigated by Wood and Dunoyer. Wood was the first to excite the sodium D-line resonance radiation by the action of the D-lines themselves. The ground state of the sodium atom is a $3^2S_{1/2}$ state. When white light is incident on the sodium, only lines in the principal series (P states) are absorbed since this is the only series ending on the ground state. However, if the excited sodium vapour is contained in a glass vessel, only the D-lines will be observed after de-excitation since the other resonance lines of the series are of wavelengths short enough to be absorbed by the glass.

A diagram of the sodium resonance cell is shown in Fig. 2.3. The shape of the cell was designed so as to eliminate two very serious defects which invariably occur in ordinary resonance cells, namely:

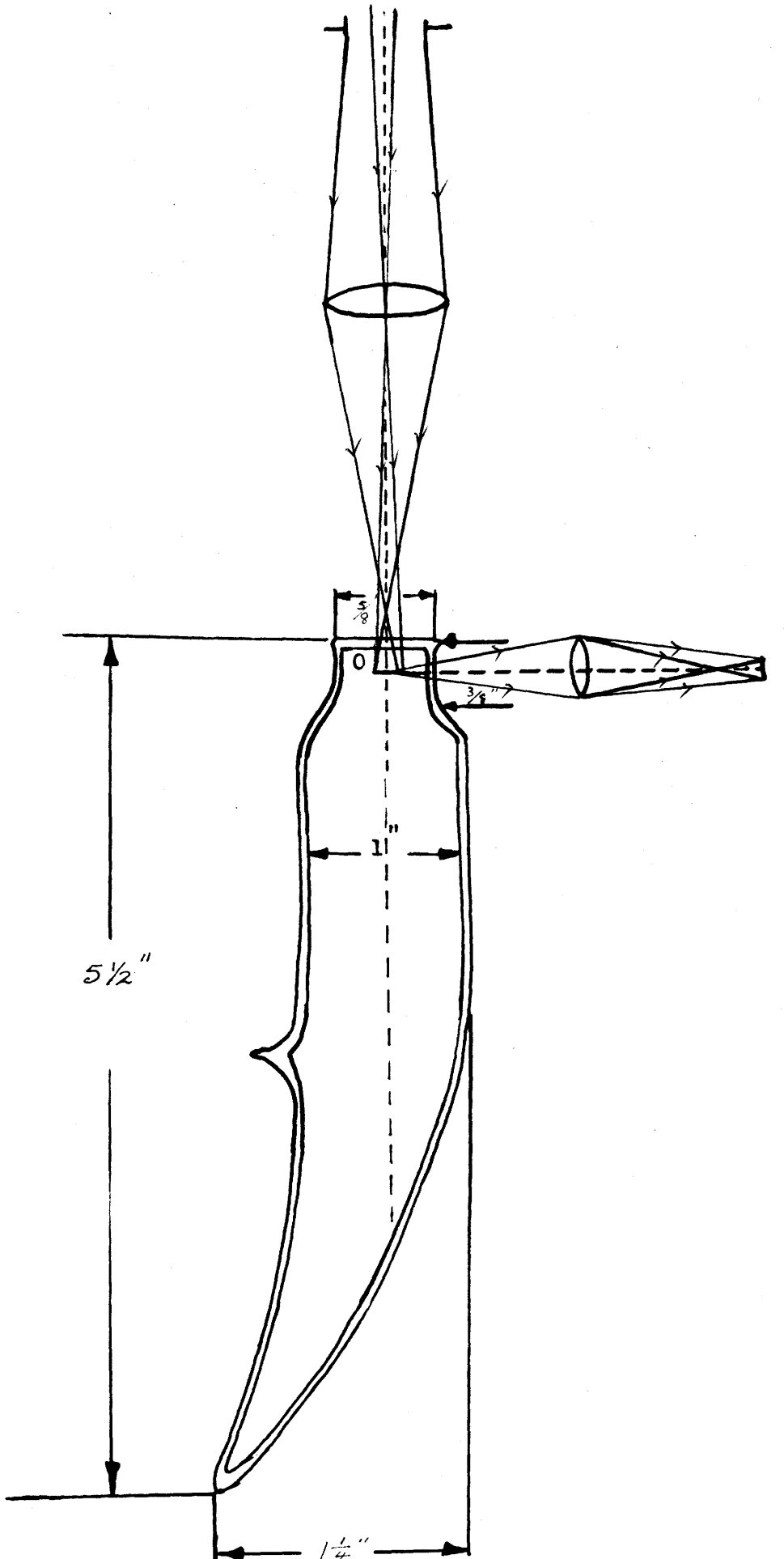

Fig. 2.3 Diagram of the sodium vapour cell showing the lens systems which image the etalon into the cell and the cell on the cathode of the photomultiplier

(1) the presence of stray light due to reflection;

(2) the presence of a layer of unexcited vapour lying between the path of the exciting beam and the window from which the resonance radiation emerges.

The image of the solar disc was produced at O by means of the optical system, and the emitted resonance radiation was observed through the side of the small tube at the exit window. The light trap prevented internal reflections, and the slight projection of the entrance window enabled the exciting beam to be confined in the region of the exit window so that the resonance radiation did not traverse the unexcited layer of vapour. The resonance cell was placed in an oven whose temperature was controlled by a temperature regulator. When using the resonance cell, it was desirable to be able to obtain substantial resonance emission to facilitate measurements. At the same time, however, it was also important to preserve a low vapour pressure (and hence low sodium density*) to minimize absorption of the resonance radiation by unexcited atoms. Thus the rear end of the tube was maintained at a temperature range of 145°-150° C., with the window end several degrees higher. This was to prevent sodium vapour from condensing on the window. Extensive baffling was necessary so as to prevent any outside stray light before the cell could be used to observe the sodium absorption lines using sunlight as the source.

*

2.4 The Calibration Lamp Unit

It was mentioned earlier that a white light source was employed in the calibration of the system. This consisted of a 500-watt Sylvania blue top projection lamp with a filament size of 1 cm. X 1 cm. The lamp was enclosed in a metal cylinder with a projecting tube containing a lens system. A diagram of the lamp unit is shown in Fig. 2.4. At the end of the projecting tube was attached a mirror M, which reflected the light into the Fabry-Perot spectrometer and the sodium cell. The lens system as shown in the diagram was designed so as to image the lamp filament at O of the sodium cell (see Fig. 2.3), the position at which the sun was imaged when using sunlight as the source. The lamp unit was attached to the side of a larger metal cylinder box containing the aperture and the 10 cm. lens. It was made adjustable so that it could be swung in and out of the aperture position during the process of making observations. As the time of observation was quite long, the lamp was constantly cooled by a fan. The air was drawn in through a bellow attached to the side of the cylinder containing the lamp. When making observations, this whole unit could be placed above the window of the Fabry-Perot spectrometer.

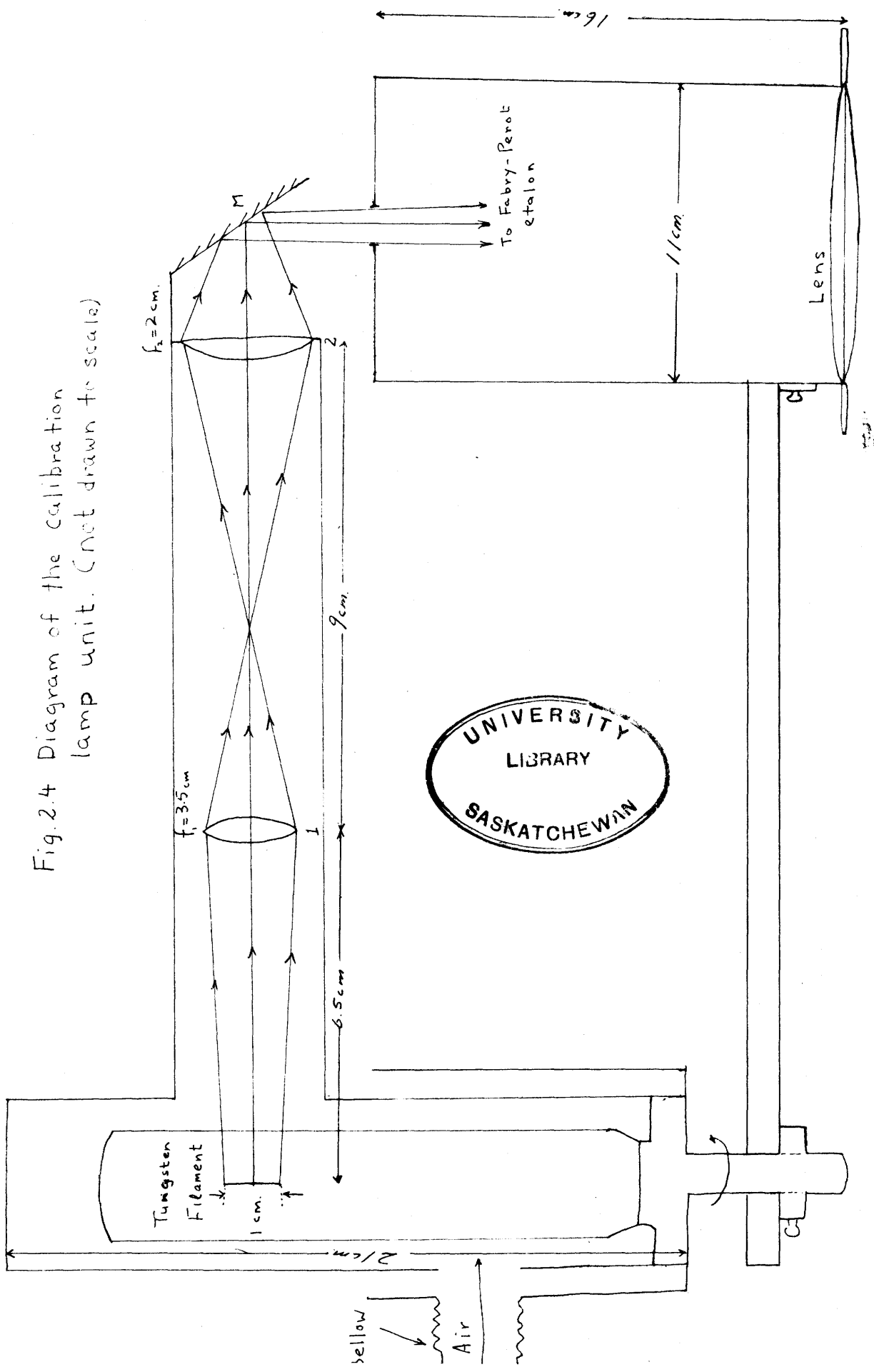

Fig. 2.4 Diagram of the calibration lamp unit. (not drawn to scale)

2.5 Instrumental Arrangement

With the exception of the coelostat, the assembled instrument is housed in room 304 of the Physics Building. The Fabry-Perot spectrometer is vibration mounted in a dexion stand, which is located under a wooden hatch. The coelostat, which is mounted on a rigid dexion platform, stands several feet above the hatch. A rectangular chimney 8" by 8" connects the hatch and the coelostat and contains a lens 10 cm. in diameter having a focal length of 106 cm.

To describe the instrument, a light beam will be followed through it. A drawing of the various components in the assembled instrument is shown in Fig. 2.5. The optical axis is vertical. In making observations, the coelostat is adjusted so as to direct a steady vertical beam of sunlight into the instrument. The beam is intercepted by a 10 cm. lens (1), which focusses the image of the sun onto the aperture (4), 0.7 cm. in diameter. A plano-convex lens (5) (f.l. 16 cm.), placed at a distance equal to its focal length behind the aperture, then forms a parallel beam of light as seen by the Fabry-Perot etalon (7). To avoid heating of the Fabry-Perot etalon, an infra-red filter (3) consisting of a 2½% $CuCl_2$ solution in a rectangular glass container is placed in front of the lens. The interference filter (6) and the Fabry-Perot etalon are contained in a cast aluminium cell.

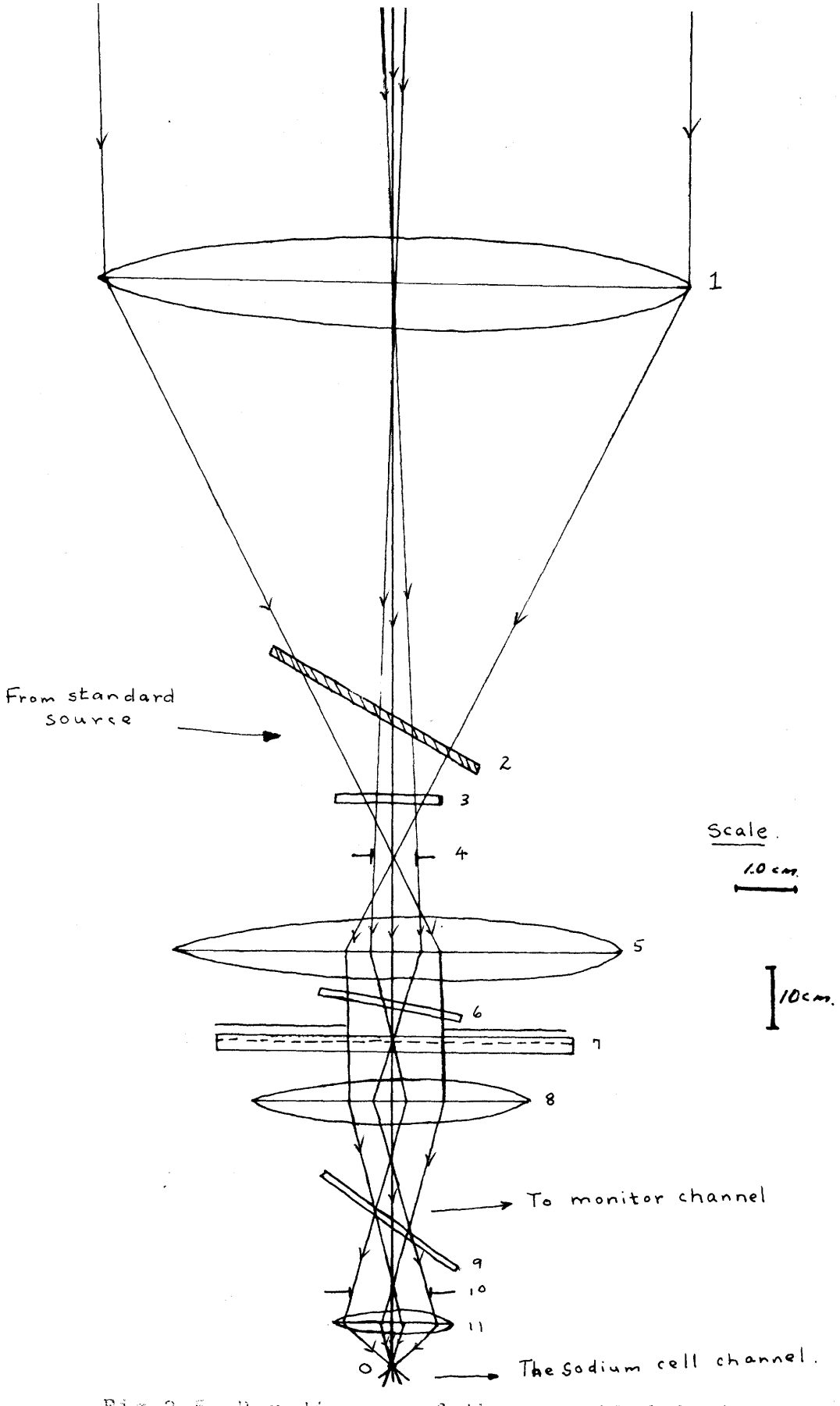

Fig. 2.5 Ray diagram of the assembled instrument (drawn to scale)

The cell is temperature controlled, as described by Shepherd (1960), so that a uniform temperature is achieved over the inner wall. This device protects the etalon and the etalon mounting from any temperature fluctuations which may destroy the plate parallelism. The interference filter is tilted by a cam mechanism and is driven by a 1 r.p.m. synchronous motor. This cam is designed to produce a sawtooth wavelength change with respect to time, and it allows the peak of its passband to be shifted to the desired wavelength. The etalon scanning is produced by a mechanical motion of the lower plate; the motion is caused by pneumatic pressure applied to an annular steel membrane. The pressure control is achieved by using a commercial current-to-pressure transducer (Minneapolis Honeywell I/P transducer). The electrical sawtooth output for the transducer is obtained from a continuous turn precision potentiometer tapped at 300° and driven by a 1 r.p.m. synchronous motor. Amplifiers are incorporated to provide the necessary current amplification for the transducer and allow adjustments of the amplitude and mean level of the sawtooth pressure signal. These electric controls enable synchronization and alignment of the passbands of the etalon and the interference filter to be obtained. Further details may be found in Zwick's M.A. thesis (1961).

The light that leaves the Fabry-Perot etalon passes

through an achromatic lens (8), 31.7 cm. focal length and 6.5 cm. diameter, mounted at the base of the aluminium cell. This lens focusses the etalon passbands into concentric fringes in its focal plane. The aperture (10) located in this focal plane allows light from only the central fringe to pass through to the sodium cell located below. The diameter of the aperture is 1.4 cm. and gives a spectral width of 5 $cm.^{-1}$ at 5893 Å. The beam-splitter (9), essentially a glass plate, reflects light into an aperture of the same size (1.4 cm.). This device makes possible simultaneous measurement of the Fraunhofer spectrum and the sodium lines scattered from the sodium cell. The first of these channels will be referred to as the monitor channel.

In the monitor channel, the light reflected by the glass plate is brought, by means of a simple optical system, to image on the photocathode of a photomultiplier (1P21) containing a preamplifier stage. The output from the preamplifier is passed through a high-frequency cut-off circuit to a final amplification stage. The final stage is an attenuator which precedes an Easterline-Angus recorder. The attenuator in this case has two positions, one having ten times as much attenuation as the other.

In the sodium cell channel, the light beam is brought into focus at O of the entrance window of the cell (see Fig.

2.3) and is scattered by the sodium vapour cell. The cell is contained in an aluminium box attached to the end of the aperture box and is temperature controlled by a temperature regulator (Scrimger, 1956). The scattered light is directed through an optical system into a detector. The complete detector unit consists of an EMI 9502b photomultiplier tube, an insulated aluminium box, a refrigerating cooling unit, and a preamplifier. This unit was kindly loaned by Dr. D. M. Hunten. The accessory electronics are housed in a metal cabinet beside the spectrometer.

To calibrate the system, a white light tungsten source (see Fig. 2.4) is used. The tungsten lamp (500 watts) and the mirror (2) are incorporated in one unit and the lamp is contained in a metal box cooled constantly by a fan. The mirror is made adjustable so that when making measurement with the sun as the source, it can be moved out away from the aperture (4). By means of an optical system, the filament of the tungsten lamp is imaged so as to fall at O, the position of the image of the sun when using sunlight as the source.

2.6 Observational Procedure

Before attempting to make observation with the Fabry-Perot spectrometer, several adjustments have to be made. The first step is to adjust the etalon and bring the plates as near parallelism as possible. This is done by means of three

spring loaded nuts, which apply pressure to and compress the invar spacers. When performing this adjustment, an Osram sodium lamp is used as the illuminating source. The second step is to synchronize the scanning of the passbands of the etalon and interference filter. Synchronization between these two scans is achieved if the etalon passband peak starts scanning when it is exactly under the passband peak of the interference filter and remains in this relative position as the filter passband scans in wavelength. The interference filter tilting mechanism fixes the starting wavelength and the linear scanning range. Hence to synchronize these two processes, the sawtooth pressure level from the output of the transducer is carefully adjusted since this controls the scanning of the etalon passbands. Synchronization is obtained when maximum transmission through the system is observed.

The standard source unit is then placed in position on top of the aluminium cell and the coelostat adjusted to direct a beam of sunlight into the instrument. An image of the sun is formed at the aperture 1, and the spectrometer is ready for observation. The temperature of the cell oven is maintained in the range 145°-150° C.

Normally, the procedure is to observe the absorption lines of the sun first. This involves one scan which lasts

60 seconds, since the interference filter and the etalon passbands make one scan in 50 seconds and recycle in 10 seconds. During this process, two spectra are produced, one in the monitor channel and the other in the sodium cell channel. The monitor channel observes the Fraunhofer spectrum; and the sodium cell channel, the scattered sodium D-lines superimposed upon the white light continuum. During the 10-second recycle, the standard source is swung into position, and a scan is taken using this as the source. This process calibrates the Fabry-Perot spectrometer and produces two spectra, one in each channel. Thus a single complete measurement takes two minutes in which four spectra are obtained. A typical sample of each type of spectrum is shown in Fig. 2.2. In the monitor channel, the scan with the tungsten lamp as the source is made with a gain ten times larger.

The results obtained by this procedure and the method of analyzing them will be presented in Chapter 4.

3. THEORY OF SOLAR ABSORPTION BY ATMOSPHERIC SODIUM

3.1 Introduction

It is known that in the atmospheres of the sun and earth, absorption processes are taking place in which solar energy is being absorbed by the outer layers of the sun and also by the earth's atmospheric constituents. These processes gives rise to the various Fraunhofer spectra of the sun as observed at the ground. In the case of sodium, the wavelengths at which the solar spectrum is absorbed are 5890 and 5896 Å--the wavelengths of the sodium D-lines.

In considering terrestrial absorption by atmospheric sodium, one must distinguish it from the absorption in the solar atmosphere; that is, the solar intensity at the bottom of the Fraunhofer lines. This quantity is not accurately known. Suppose p_0 denotes the residual intensity at the bottom of the Fraunhofer lines with no absorption by terrestrial sodium and p with absorption by sodium (Fig. 3.1), we can obtain an equation governing the absorption process by considering a column of atmosphere of unit cross-section containing N atoms along the path of the solar beam and having

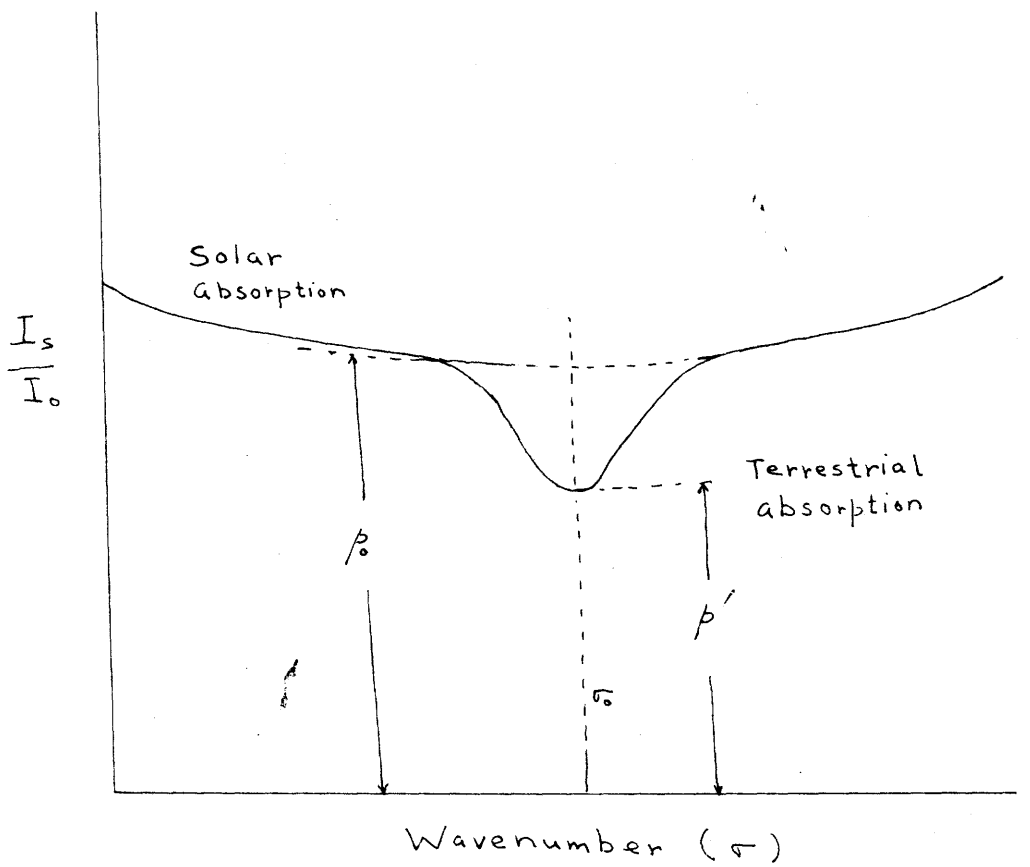

Fig. 3.1 Intensity distribution at the bottom of one of the Fraunhofer D-lines showing the terrestrial sodium absorption.

an absorption coefficient per atom denoted by k. The equation is

$$p = p_0 e^{-kN} \qquad \ldots (3.1)$$

At the centre of the line, however,

$$p' = p_0 e^{-k_0 N} \qquad \ldots (3.2)$$

where k_0 is defined for the centre of the line. Sometimes this will be written as

$$p' = p_0 e^{-\tau_0} \qquad \ldots (3.3)$$

where τ_0 is the optical thickness at the centre of the line.

The sodium D-lines, however, possess hyperfine structures, and these must be accounted for in considering the absorption of solar energy by the terrestrial sodium. The D_1 line has four hyperfine components (hfs) while the D_2 line has six. These hyperfine components result from the interaction of the electron and nuclear magnetic moments. The various hyperfine components of the sodium D-lines and their wavenumbers and level-separations are shown in Fig. 3.2 (McNutt and Mack, 1963). Since the separations of the P-levels are very narrow, each line is effectively divided into two hyperfine groups of fine structure lines. These hyperfine groups may be labelled D_{1a}, D_{1b}, D_{2a}, and D_{2b}. Doppler

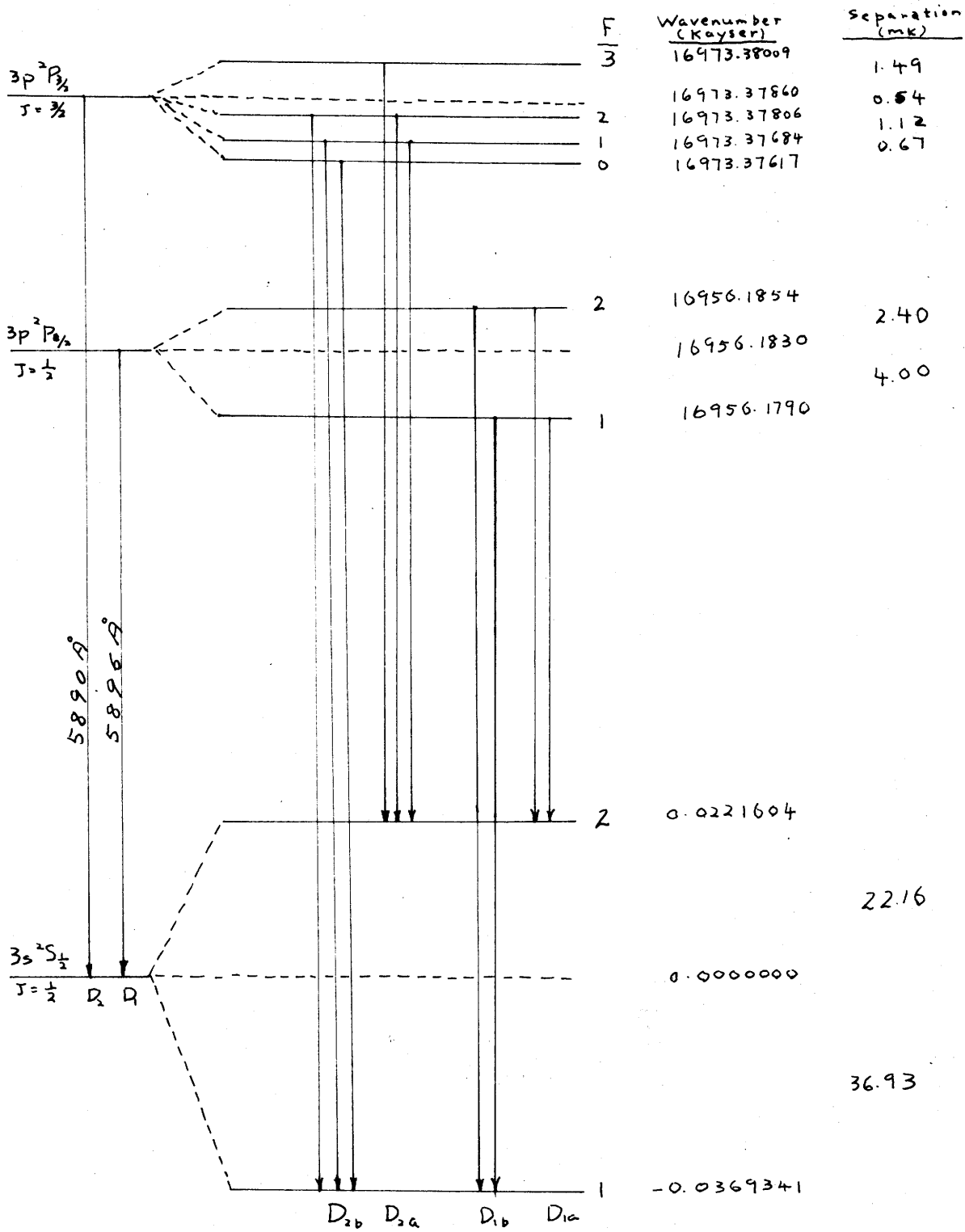

Fig. 3.2 Energy levels of the 3s and 3p configurations of Na, showing hyperfine structures for nuclear spin $I = \frac{3}{2}$. Total angular momentum $F = (J+I), (J+I-1), \ldots\ldots (J-I)$.

broadening at the temperature of the sodium layer (200°-250° K.) effectively blends together the hfs lines within one group without much overlapping of the profiles between different groups (Chamberlain, Hunten, and Mack, 1958a). A diagram illustrating the situation is shown in Fig. 3.3. This diagram is taken from Chamberlain (1961).

A detailed theory of the sodium absorption, taking into account the two hyperfine groups and the temperature profiles of atmospheric D-lines (200° K.) and the D-lines scattered by the sodium cell (400° K.), will be considered in the next section. The method of evaluating the effective absorption coefficient denoted by $\bar{k}$ and the measuring procedure are described in sections 3.3 and 3.4.

3.2 Theory of Sodium Absorption

In considering the solar absorption by atmospheric sodium, one needs to take into account the hyperfine groups of each D-line. As mentioned earlier, in the upper atmosphere each D-line is divided into two hyperfine groups, which have been labelled as D_{1a}, D_{1b}, D_{2a}, and D_{2b} for the D_1 and D_2 lines respectively. The temperature profiles of the atmospheric D-lines (200° K.) and the scattered D-lines from the sodium cell (400° K.) (see Fig. 3.3) will be taken into account in the theory.

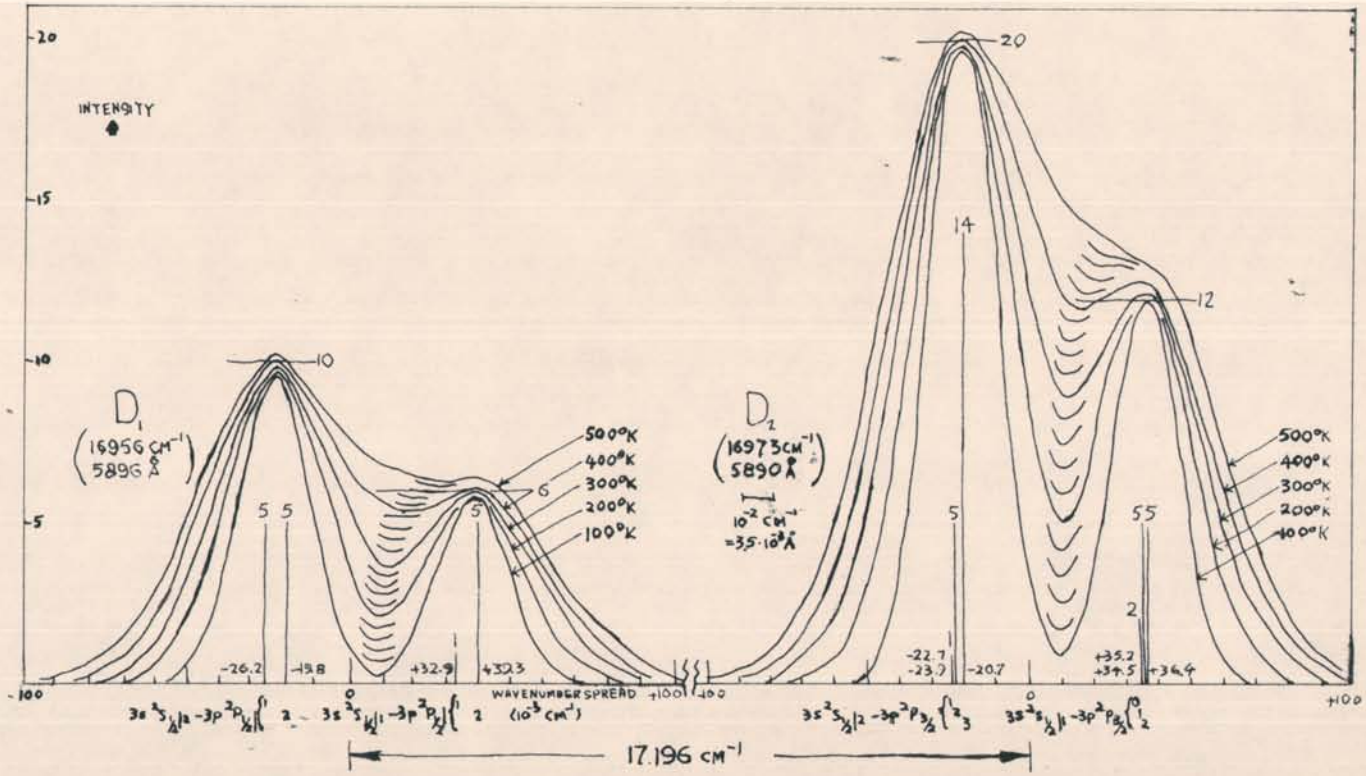

SODIUM RESONANCE LINE SHAPES AT DIFFERENT TEMPERATURES

FIG. 3.3 Line profiles for D_1 and D_2 emission at various temperatures. From Chamberlain, Hunten, and Mack [1958a].

To avoid complexity, only a single line (D_1 or D_2) will be considered. Suppose $I_S(\sigma)$ (Fig. 3.4a) is the solar intensity incident on the atmosphere and $I_T(\sigma)$ the solar spectrum after transmission through the atmosphere (Fig. 3.4b), then the equation governing the absorption is

$$I_T(\sigma) = I_S(\sigma)e^{-k_T N_T} \qquad \ldots (3.4)$$

where k_T is the absorption coefficient for a 200° K. sodium profile. After this the solar beam is passed through the Fabry-Perot spectrometer and the beam is split into two paths by the glass plate, one entering the monitor channel while the other the sodium cell.

In the monitor channel, let Y_{TM} (Fig. 3.4c) be the recorded signal after transmission of I_T through the Fabry-Perot etalon whose passband shape is denoted by $W(\sigma)$. When spectrum passband is at σ, the intensity transmitted at σ' will be $I_T(\sigma')W(\sigma' - \sigma)$ and the intensity through the whole passband will then be $\int_{-\infty}^{\infty} I_T(\sigma')W(\sigma' - \sigma)d\sigma'$. The recorded signal will be

$$Y_{TM}(\sigma) = L_M \int_{-\infty}^{\infty} I_T(\sigma')W(\sigma' - \sigma)d\sigma' \qquad \ldots (3.5)$$

where L is the luminosity of the Fabry-Perot spectrometer defined as the ratio of the output signal to source intensity.

To obtain the intensity seen by the cell, it would be

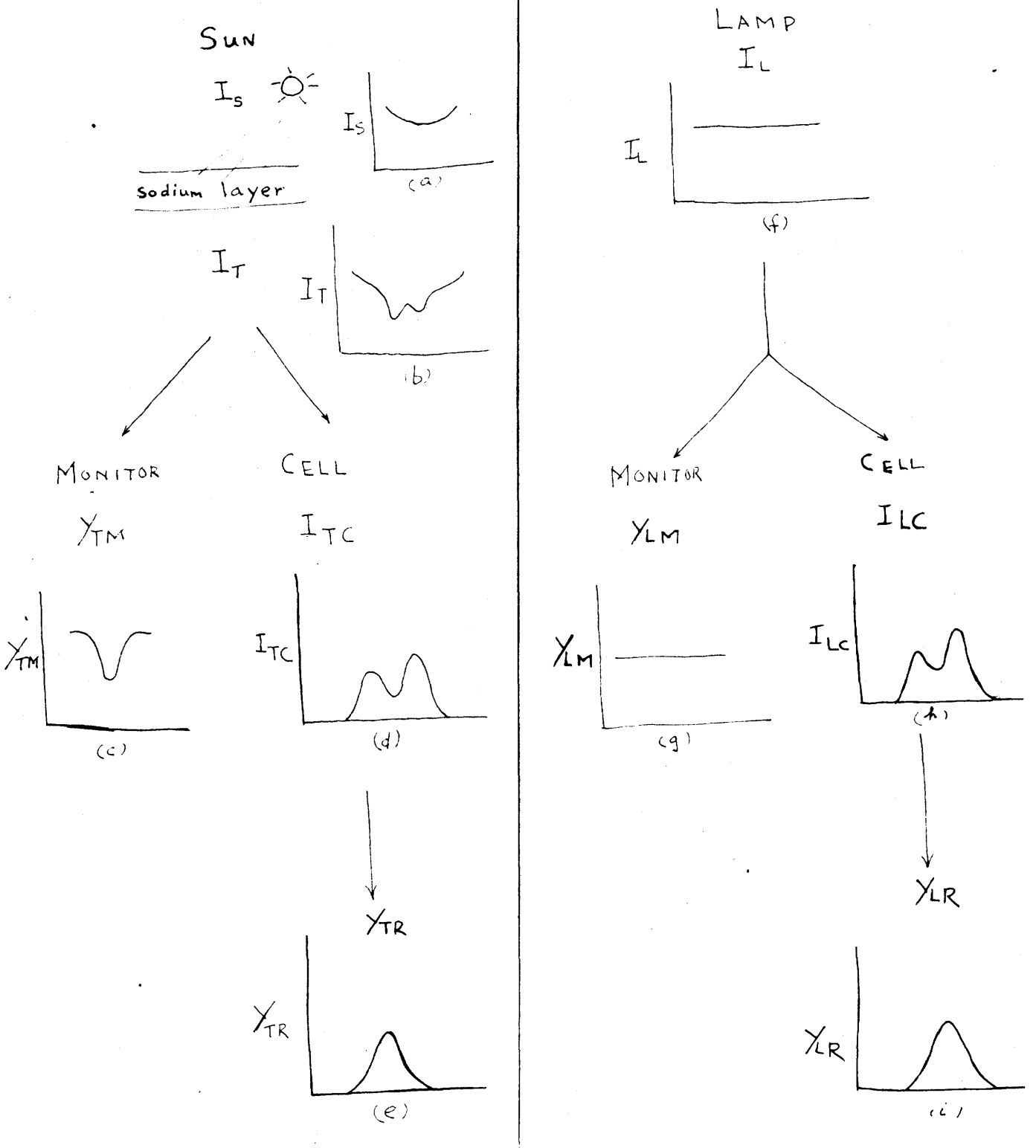

Fig. 3.4 Diagram showing the step-by-step analysis by the instrument of a single D-line, and the corresponding symbols used in the calculations.

easier to consider the cell as being placed before the Fabry-Perot etalon. Hence, if I_{TC} (Fig. 3.4d) denotes the spectrum after scattering by the 400° K. sodium profile, then

$$I_{TC} = cI_T(1 - e^{-k_C N_C}) \qquad \ldots (3.6)$$

where c is a sort of scattering function for the sodium vapour cell. However, after passing through the Fabry-Perot, the recorded signal Y_{TR} (Fig. 3.4e) is given by the following relation

$$Y_{TR}(\sigma) = L_R \int_{-\infty}^{\infty} I_{TC}(\sigma')W(\sigma' - \sigma)d\sigma' \qquad \ldots (3.7)$$

In calibrating the system, a white light source is used. Let I_L be the incident lamp spectrum (Fig. 3.4f). Hence in the monitor channel, the recorded signal Y_{LM} (Fig. 3.4g) is

$$Y_{LM}(\sigma) = L_M \int_{-\infty}^{\infty} I_L(\sigma')W(\sigma' - \sigma)d\sigma' \qquad \ldots (3.8)$$

and in the cell channel, we have I_{LC} (Fig. 3.4h), where

$$I_{LC} = cI_L(1 - e^{-k_C N_C}) \qquad \ldots (3.9)$$

and the recorded signal Y_{LR} (Fig. 3.4i) is

$$Y_{LR}(\sigma) = L_R \int_{-\infty}^{\infty} I_{LC}(\sigma')W(\sigma' - \sigma)d\sigma' \quad . \ . \ . \ (3.10)$$

It is now necessary to relate the above quantities to the ones which are measured in the experiment. The monitor channel gives a constant reading with the lamp as source; this is denoted by B_L in Fig. 2.2(d) on page 9. Similarly, with the sun as source a deflection B_S is obtained as shown in Fig. 2.2(c). Allowance must be made for the Fraunhofer lines, but the description of the procedure will be left until later. Hence we can identify $Y_{LM}(\sigma)$ with B_L and Y_{TM}(background) with B_S. Ordinarily one would have to consider gain factors and units, but as will be seen later, these will be self-cancelling and so may be neglected.

For the cell channel, consider equation 3.7 for the recorded signal with the sun as source:

$$Y_{TR}(\sigma) = L_R \int_{-\infty}^{\infty} I_{TC}(\sigma')W'(\sigma' - \sigma)d\sigma'$$

It can be shown* that for a convolution integral such as the above, the area under the function Y_{TR} is equal to the product of the area under the curves. Hence, in terms of areas,

$$Y'_{TR} = L_R I'_{TC} W' \quad . \ . \ . \ (3.11)$$

---

*Chabbal (1953).

and $$Y'_{LR} = L_R I'_{LC} W'$$

where it is understood that from now on these primed symbols represent areas.

We now have $$Y_{LM} = B_L$$
$$Y_{TM} = B_S$$
$$Y'_{TR} = L_R I'_{TC} W'$$
and $$Y'_{LR} = L_R I'_{LC} W'.$$

The shapes of Y_{TR}, Y_{LR}, and W will all be the same, since the half-width of W dominates the others. Hence one need only measure peak heights of Y_{TR} and Y_{LR} since they are proportional to the areas Y_{TR} and Y_{LR}. That is, except for proportionality constants which will cancel later, we can identify Y_{LR} with D_L and Y_{TR} with D_S (D_S is d_S after correction for the Fraunhofer lines; D_L and d_S are shown in Fig. 2.2).

We can obtain an 'effective' residual intensity p_e by taking the ratio $\frac{D_S}{B_S}$ times the calibration factor $\frac{B_L}{D_L}$ giving

$$p_e = \frac{D_S}{D_L} \cdot \frac{B_L}{B_S} \qquad \ldots (3.13)$$

This quantity can be measured experimentally. Then, to deduce the abundance N from observed p_e, we must perform integrations numerically. Theoretically, p_e can be written

$$p_e = \frac{I'_{TC}}{I'_{LC}} \cdot \frac{B_L}{B_S} \qquad \ldots (3.14)$$

Substituting for I'_{TC} and I'_{LC},

$$p_e = \frac{B_L}{B_S} \times \frac{\int_{-\infty}^{\infty} I_{TC}(\sigma)d\sigma}{\int_{-\infty}^{\infty} I_{LC}(\sigma)d\sigma} \qquad \ldots (3.15)$$

This can be written as follows

$$p_e = \frac{B_L}{B_S} \frac{c\int_{-\infty}^{\infty} I_S e^{-k_T N_T}(1 - e^{-k_C N_C})d\sigma}{c\int_{-\infty}^{\infty} I_L(1 - e^{-k_C N_C})d\sigma}$$

$$= \frac{B_L}{B_S} \frac{I_O}{I_L} \frac{\int_{-\infty}^{\infty} \frac{I_S}{I_O} e^{-k_T N_T}(1 - e^{-k_C N_C})d\sigma}{\int_{-\infty}^{\infty}(1 - e^{-k_C N_C})d\sigma} \qquad \ldots (3.16)$$

where I_L and I_O are constants. The term $e^{-k_C N_C}$ may be written in terms of a power series; i.e.,

$$e^{-k_C N_C} = 1 - k_C N_C + \frac{(k_C N_C)^2}{2!} - \cdots \qquad \ldots (3.17)$$

Since $k_C N_C$ is very small, a good approximation is obtained by taking the first two terms in (3.17). Therefore, equation (3.16) can be written as

$$p_e = \frac{B_L}{B_S} \times \frac{I_O}{I_L} \frac{\int_{-\infty}^{\infty} \frac{I_S}{I_O} e^{-k_T N_T k_C N_C d\sigma}}{\int_{-\infty}^{\infty} k_C N_C d\sigma} \quad \ldots (3.18)$$

We shall write this in the form

$$p_e = p_O e^{-\bar{k} N_T} \quad \ldots (3.19)$$

where $\bar{k}$ is the effective absorption coefficient for the D-lines. Once $\bar{k}$ has been calculated, reduction of data can be made simply by using these $\bar{k}$ values.

3.3 Evaluation of the Effective Absorption Coefficient $\bar{k}$

Equation (3.20) provides a means of evaluating the effective coefficient $\bar{k}$ numerically. In the numerical evaluation, the integral is replaced by a summation; i.e., equation (3.18) becomes

$$p_e = \frac{B_L}{B_S} \cdot \frac{I_O}{I_L} \cdot \frac{\sum_{n=1}^{n} \frac{I_S}{I_O} e^{-k(\sigma_O + n\Delta\sigma) N_T k_C N_C \Delta\sigma}}{\sum_{n=1}^{n} k_C N_C \Delta\sigma} \quad (3.20)$$

Since N_C can be assumed to be constant, it can be dropped from the equation.

From $p_e = p_O e^{-\bar{k} N_T}$ (see equation 3.19) when $N_T \longrightarrow 0$, $p_e \longrightarrow p_O$.

Therefore from equation (3.20), when $N_T \longrightarrow 0$, p_O is given by the expression

$$p_O = \frac{B_L}{B_S} \cdot \frac{I_O}{I_L} \cdot \frac{\sum_{n=1}^{n} \frac{I_S}{I_O} k_C}{\sum_{n=1}^{n} k_C} \quad \ldots (3.21)$$

Therefore from equation (3.20),

$$p_e = p_O \frac{\sum_{n=1}^{n} \frac{I_S}{I_O} e^{-k_T(\sigma_O + n\Delta\sigma)N_T} k_C \Delta\sigma}{\sum_{n=1}^{n} \frac{I_S}{I_O} k_C \Delta\sigma} \quad \ldots (3.22)$$

Comparing equations (3.19) and (3.22),

$$e^{-\bar{k}N_T} = \frac{\sum_{n=1}^{n} \frac{I_S}{I_O} e^{-k_T(\sigma_O + n\Delta\sigma)N_T} k_C \Delta\sigma}{\sum_{n=1}^{n} \frac{I_S}{I_O} k_C \Delta\sigma} \quad \ldots (3.23)$$

By evaluating the expression on the right-hand side numerically, one can obtain $\bar{k}$. The procedure adopted was to divide the 200° K. temperature profile of the hyperfine groups of the D-lines into n number of equal wavenumber intervals as shown in Fig. 3.5. In order to obtain the

absorption coefficient k for each wavenumber, the scale of intensity in the original diagram (Chamberlain, 1961) was converted into that of absorption coefficient using a reduction factor. The reduction factor was obtained by using the effective value of the absorption coefficient at the centre of the D-line as calculated by Chamberlain (1961) and dividing this value by the ordinate at the centre of the line as on the graph. In this case, the D_{1a} line was used. The calculated value of the effective absorption coefficient at the centre of this line is 4.35 (Chamberlain, 1961) while the ordinate on the graph is 9.60. Hence the absorption

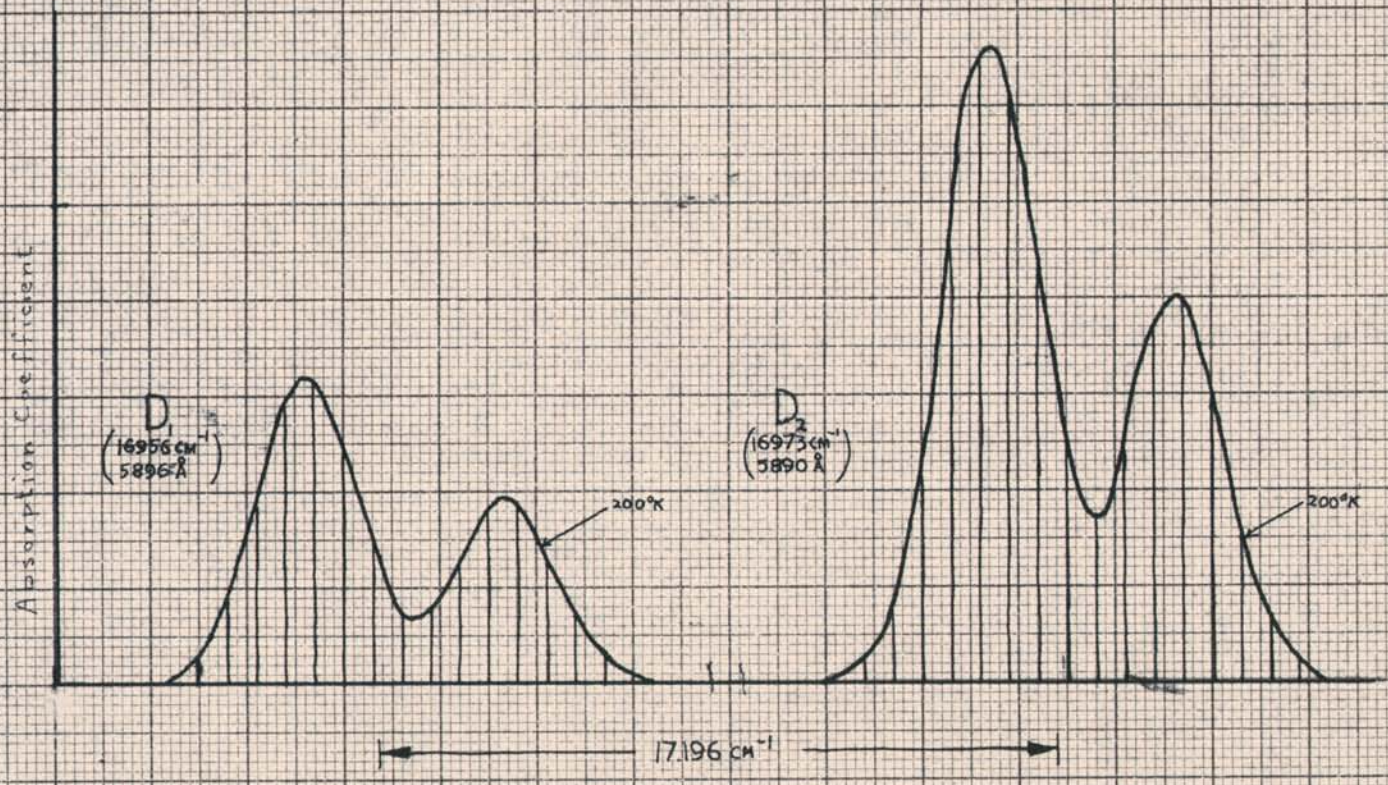

FIG. 3.5 Line profiles for D_1 and D_2 emission at 200° K (From Chamberlain, Hunten, and Mack [1958a])

coefficient for each wavenumber can be obtained simply by multiplying the ordinate as obtained on the graph by the reduction factor $\frac{4.35}{9.60}$. For a fixed value of sodium abundance, the exponential term for each wavenumber can be calculated. Each value was then multiplied by the corresponding value of $\frac{I_S}{I_O}$, which was obtained from the recent work of McNutt (1962). McNutt, in his work on terrestrial absorption by atmospheric sodium, obtained two equations governing the solar D_1 and D_2 line profiles. The equations are as follows.

For D_1-line,

$$I_S = I_O e^{\left(\frac{\bar{\nu}}{\bar{\nu}_e}\right)^A} \qquad \ldots (3.24)$$

where $\bar{\nu}_e$ = 217 mK and A = 2.15.

For D_2-line,

$$I_S = I_O e^{\left(\frac{\bar{\nu}}{\bar{\nu}_e}\right)^A} \qquad \ldots (3.25)$$

where $\bar{\nu}_e$ = 227 mK and A = 2.13. The wavenumber of each ordinate of the hyperfine groups of each D-line as shown in Fig. 3.5 was inserted in the respective equations above, and each value of $\frac{I_S}{I_O}$ was calculated. This value was then multiplied by the corresponding value of $e^{-k_T N_T}$ previously obtained. The resultant value for each wavenumber was plotted against the corresponding wavenumber. The graphs obtained were those of the sodium D-lines after transmission

through the sodium layer as shown in Fig. 3.6a and b for abundances of 8 X 10^9 to 50 X 10^9 atoms/cm.^{2} column.

Each quantity $\frac{I_S}{I_O} e^{-k_T N_T}$ obtained was then multiplied by the corresponding value of k_C, where k_C is the absorption coefficient of the 400° K sodium profile. The value of k_C for each wavenumber was normalized in the same way as k_T but using a reduction factor of $\frac{4.35}{10}$ (see Fig. 3.7). The n values obtained after multiplication were summed and divided by the sum of the n values of k_C. This completed the evaluation of the right-hand side of equation (3.23). Hence for different values of sodium abundances, the effective absorption coefficient $\bar{k}$ can be evaluated. Table 3.1 shows a set of $\bar{k}$ values using abundances varying from 10 X 10^9 to 50 X 10^9 atoms/cm.^{2} column. Plots of $\bar{k}N_T$ against N_T for the D_1 and D_2 lines were obtained, and the graphs are shown in Figs. 3.8a and b. The graphs turned out to be straight lines. However, it was noticed that for abundances below 10 X 10^9 atoms/cm.^{2} column, the calculations became most critical.

3.4 The Measuring Procedure

As stated before, the device used in this experiment to measure the solar absorption by atmospheric sodium is a low-resolution Fabry-Perot spectrometer coupled to a sodium resonance cell operated at a fixed temperature. The spectrometer resolved the sodium D_1 and D_2 lines, which were then

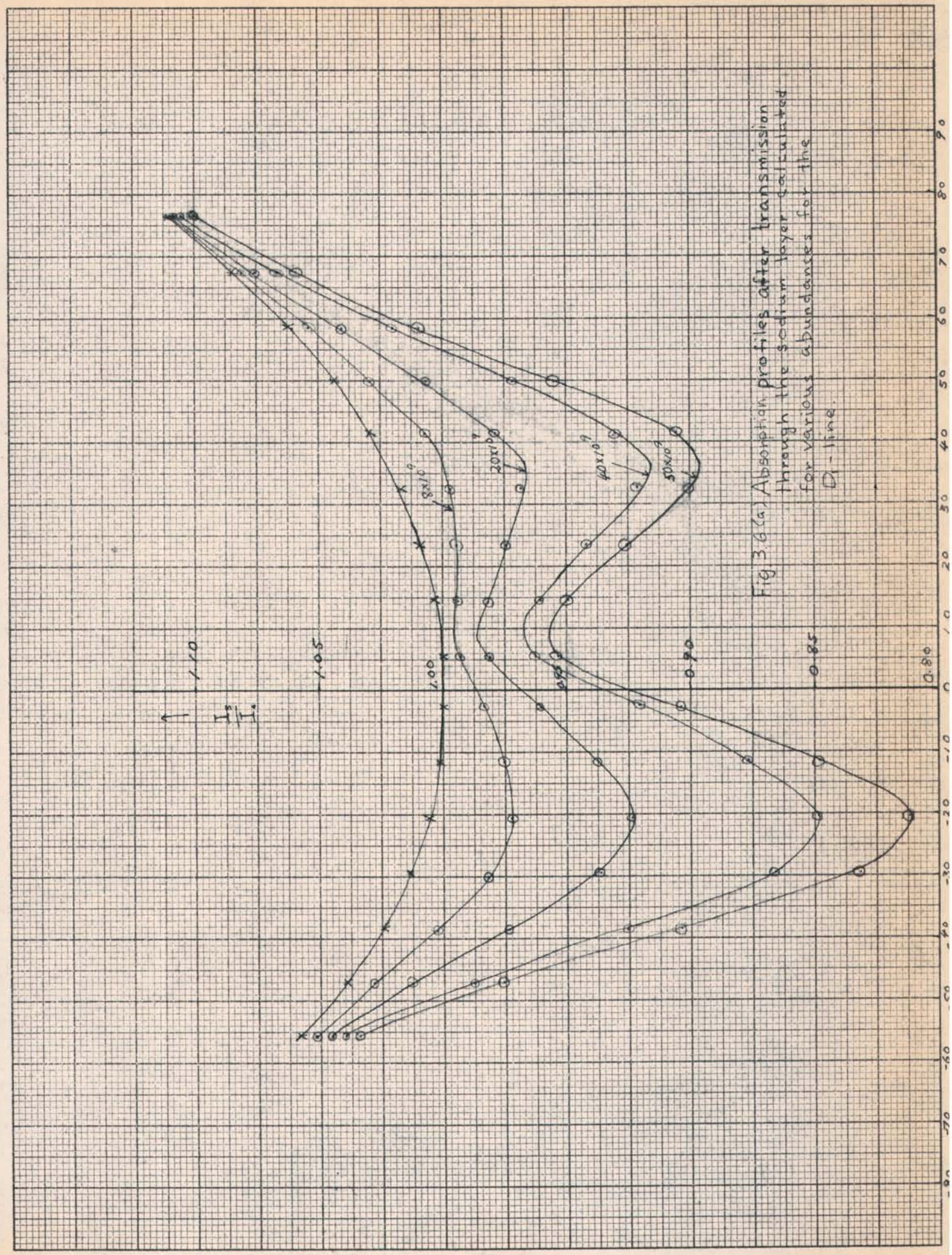

Fig 3.6(a) Absorption profiles after transmission through the sodium layer calculated for various abundances for the D - line.

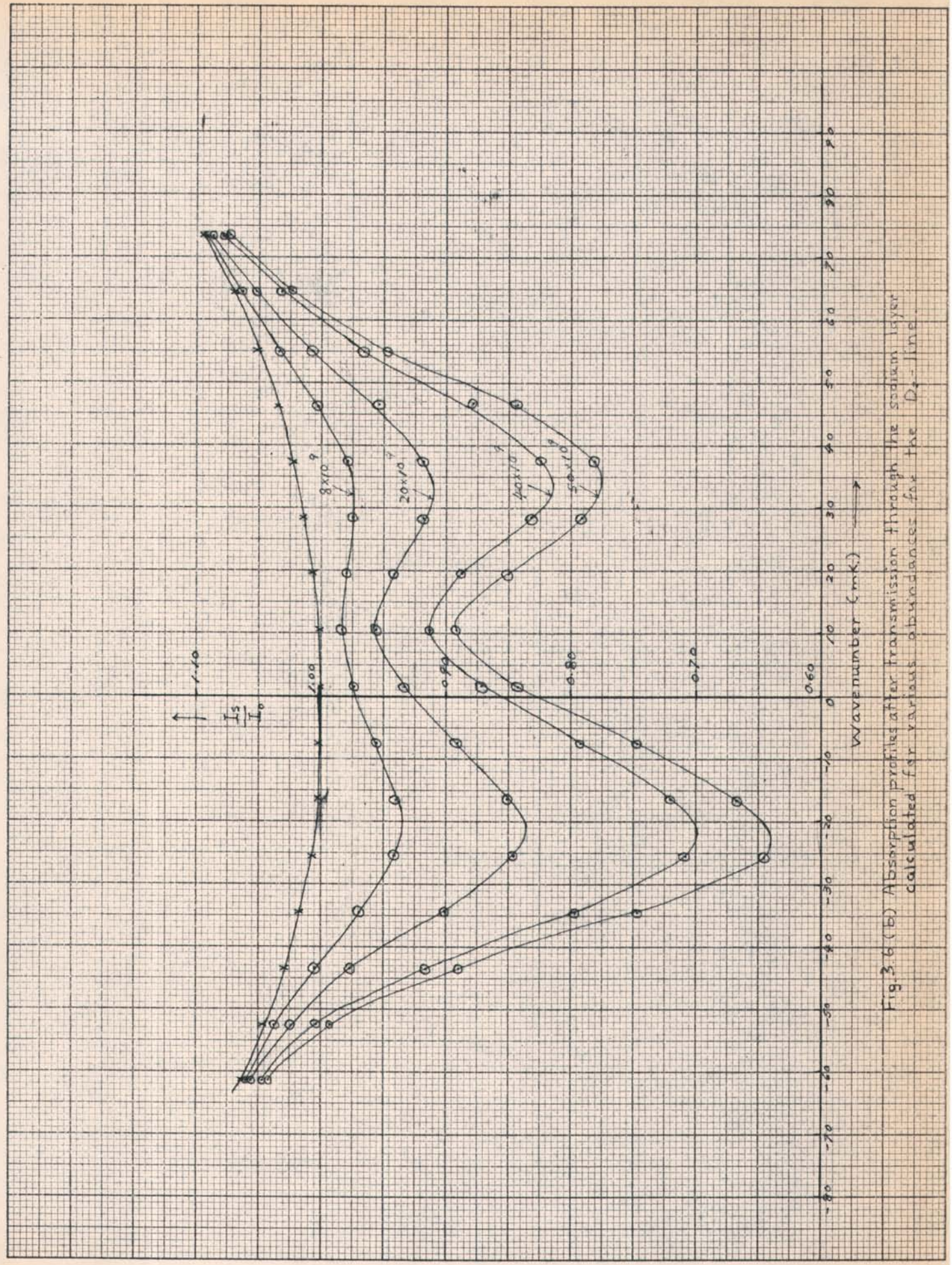

Fig. 3.6 (b) Absorption profiles after transmission through the sodium layer calculated for various abundances for the D_2 line

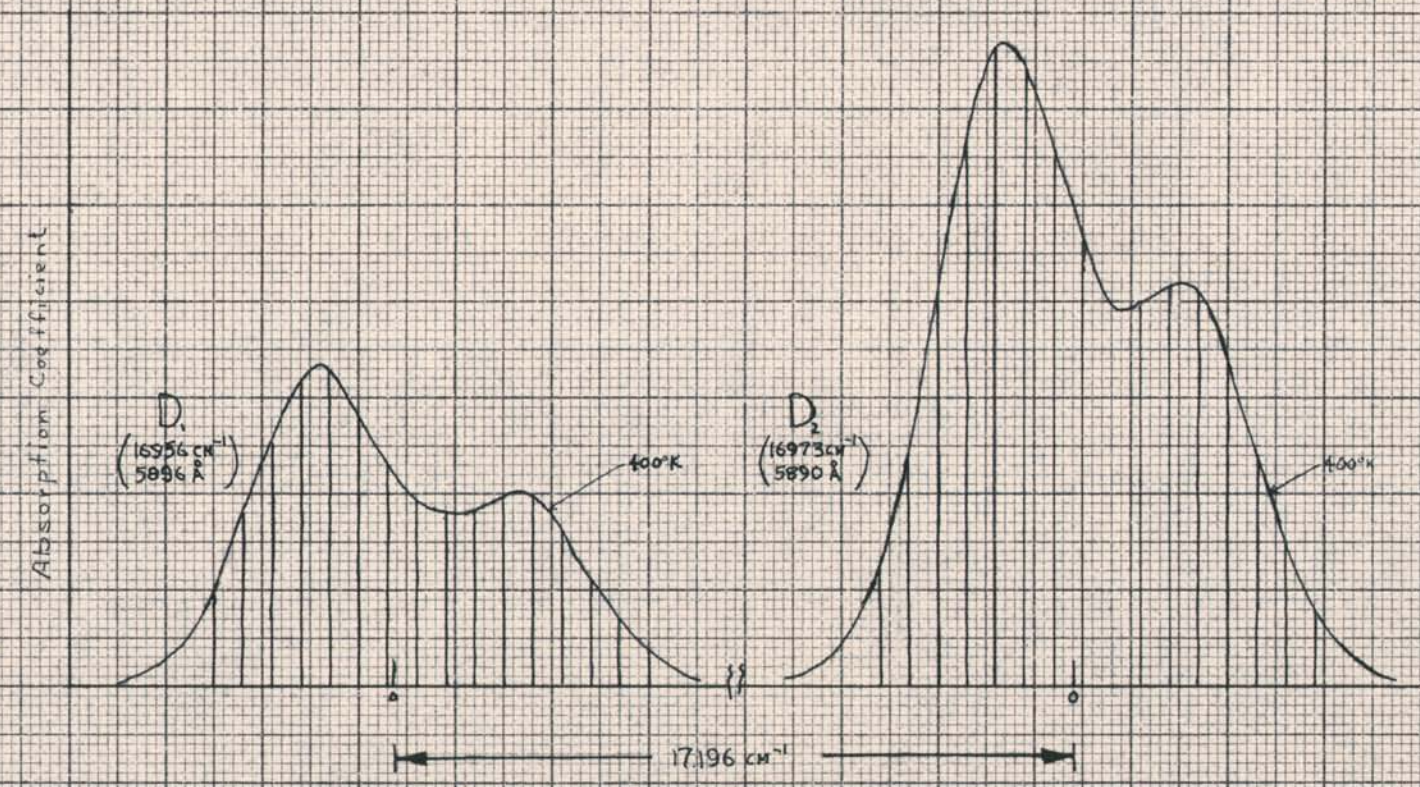

FIG. 3.7 Line profiles for D_1 and D_2 emission at 400°K. (From Chamberlain, Hunten, and Mack [1958a])

TABLE 3.1

THE EVALUATED EFFECTIVE ABSORPTION COEFFICIENT $\bar{k}$

$N_T \div 10^9$ (atoms/cm.^{2} column)	$\bar{k} \div 10^{-12}$ (D_1) (cm.^{2})	$\bar{k} \div 10^{-12}$ (D_2) (cm.^{2})	$\bar{k}N_T \div 10^{-2}$ (D_1)	$\bar{k}N_T \div 10^{-2}$ (D_2)	$\frac{\bar{k}(D_1)}{\bar{k}(D_2)}$
1.0	2.50	4.30	0.25	0.43	0.58
4.0	2.25	4.83	0.90	1.93	0.47
8.0	2.35	4.68	1.88	3.74	0.50
16.0	2.40	4.78	3.84	7.65	0.51
20.0	2.32	4.77	4.63	9.53	0.49
30.0	2.35	4.73	7.06	14.20	0.50
40.0	2.29	4.70	9.18	18.81	0.49
50.0	2.31	4.68	11.57	23.42	0.50

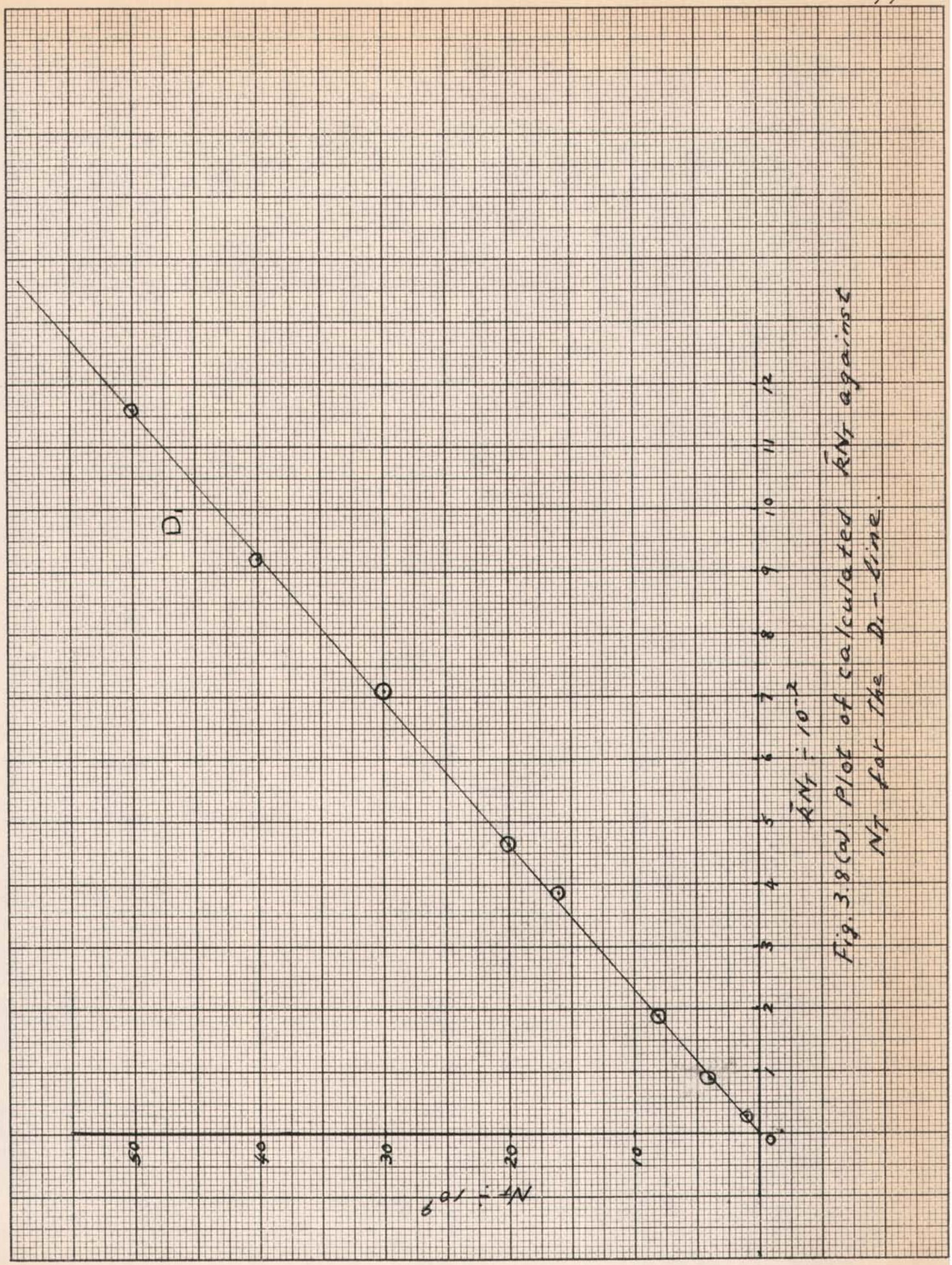

Fig. 3.8(a) Plot of calculated $\bar{K}N_T$ against N_T for the D - Line.

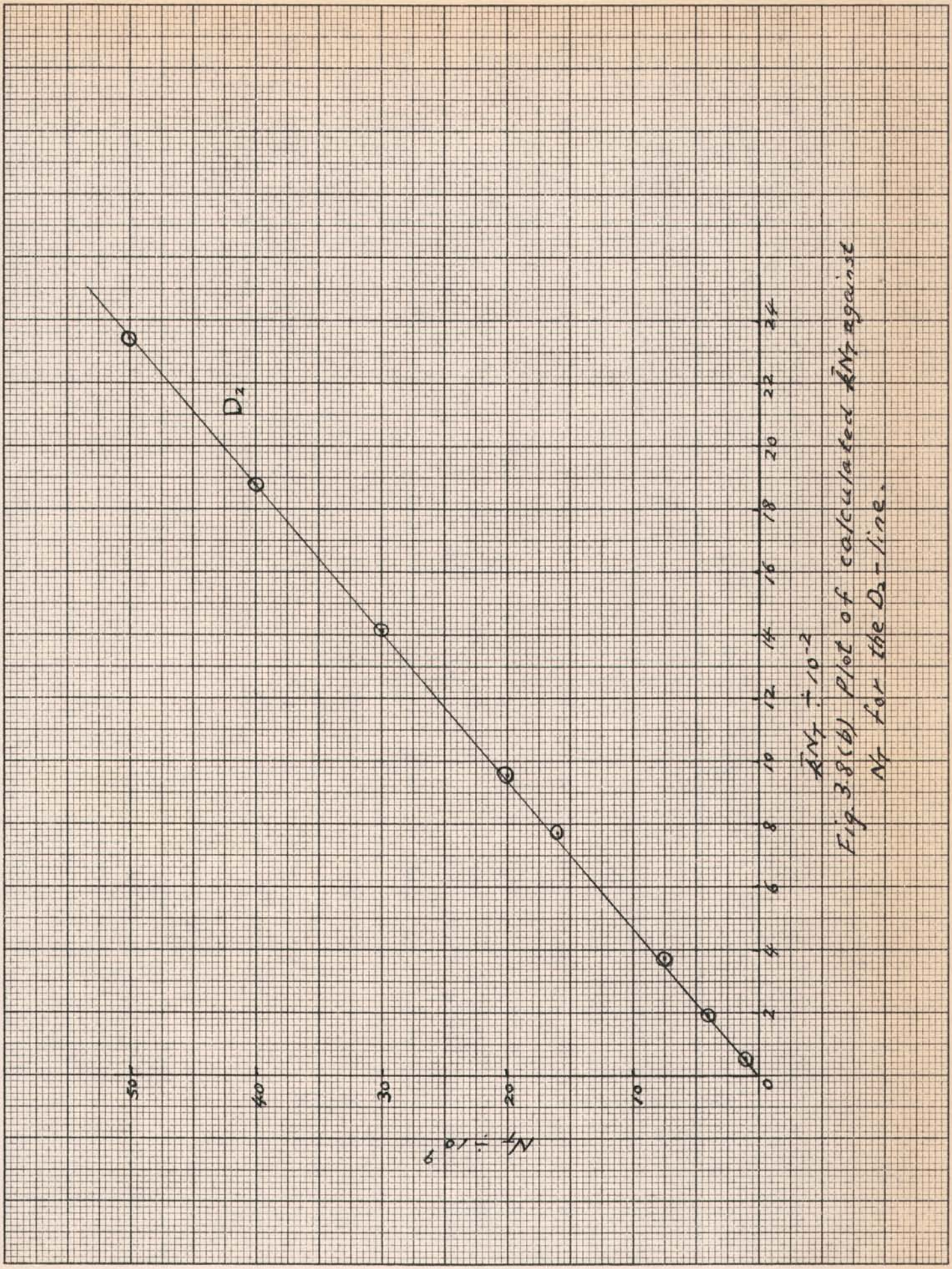

Fig. 3.8(b) Plot of calculated $\bar{R}N_T$ against N_T for the D_2-line.

scattered from the sodium vapour cell into a detector. Each type of spectrum obtained during observation was shown in Fig. 2.2.

In Chapter 3 it was shown that equation (3.21) governed the terrestrial absorption of solar radiation by sodium; i.e.,

$$p_e = p_o e^{-\bar{k}N_T}$$

Replacing N_T by N sec.$\propto$, where N refers to vertical sodium abundance, we have

$$p_e = p_o e^{-\bar{k}N \sec.\propto} \qquad \ldots (3.26)$$

and from equation (3.13)

$$p_e = \frac{D_S \times B_L}{D_L \times B_S} \qquad \ldots (3.27)$$

where B_S is chart deflection recorded using the sun as the source and is proportional to Y'_{BM} and D_L, B_L the chart deflection recorded using the calibration lamp and

proportional to Y'_{LR} and Y'_{LM}. These quantities are shown in Fig. 2.2. The quantity D_S refers to the corrected chart deflection of the D-lines. A correction is necessary, since when using sunlight to illuminate the sodium cell, the depth of the Fraunhofer lines in the background (see Fig. 2.2a) could not be readily measured. This quantity must be known if the true values of the D-line intensities were to be obtained, since these intensities must be measured from the troughs of the observed Fraunhofer lines rather than from the level of the continuum. Spectrum (c) enabled the fractional depth of the Fraunhofer lines, denoted by q, to be obtained. Hence the corrected D-line intensity recorded using the sun as the source is

$$D_S = d_S + qb_S \qquad \ldots (3.28)$$

Hence the equations to be used in the evaluation of p_e are as follows: For the D_1-line,

$$p_{e1} = \frac{D_{S1} \times B_L}{D_{L1} \times B_S} \qquad \ldots (3.29a)$$

and for the D_2-line,

$$p_{e2} = \frac{D_{S2} \times B_L}{D_{L2} \times B_S} \qquad \ldots (3.29b)$$

From equation (3.26), for each sodium line,

$$p_e = p_0 e^{-\bar{k}N \sec.\alpha}$$

Taking logarithm,

$$\begin{aligned} \ln p_e &= \ln p_0 - \bar{k}N \sec.\alpha \\ &= \ln p_0 - \tau_e \sec.\alpha \end{aligned} \qquad \ldots (3.30)$$

where $\tau_e = \bar{k}N$ is the effective optical thickness of the sodium D-lines.

The measurement of the p_e values by equations (3.29a and b) for different values of sec.α --i.e., from sunrise to noon or noon to sunset--was done experimentally. A plot of ln p_e against sec.α should then yield a negative slope, which would measure τ_e, the optical thickness of the sodium layer. By using the relation $\tau_e = \bar{k}N$ and the effective absorption coefficient $\bar{k}$, the vertical abundance N could be determined. At the same time, the values of p_0 could be obtained by extrapolating the graphs to sec.α = 0, which assumes no terrestrial absorption by sodium.

4. RESULTS

4.1 Introduction

The Fabry-Perot spectrometer in conjunction with the sodium resonance cell as described in Chapter 2 was used to observe the terrestrial absorption by sodium during the period of January, February, March, April, and July. As mentioned earlier, the observational technique involved using a coelostat to direct a steady beam of sunlight into the instrument. The Fabry-Perot spectrometer was made to scan for one minute during which two spectra were produced, one in each channel. In the cell channel, the resonance emission lines were observed while in the monitor channel the Fraunhofer spectrum of the sodium D-lines was obtained. These two spectra were shown respectively as spectra (a) and (c) in Fig. 2.2. After this, the tungsten white light source was used to calibrate the system. During this process, two more spectra were produced, one in each channel, shown as spectra (b) and (d) in Fig. 2.2. Thus a complete single measurement took two minutes. However, a day's run normally took three to five hours, either in the morning or in the afternoon, in

order to obtain a substantial change in the value of sec.α. Successful observations were made during the above-mentioned period, but owing to the fact that exceptionally clear skies were required for observation, an average of two to three runs could only be made during each month. Altogether, a total of thirteen runs were made on eleven different days. The data obtained during each run, after analysis, yielded a value for the sodium abundance N, the number of absorbing atoms per vertical column of unit cross-section area, and also, as a by-product, the value of the residual intensities of the sodium D-lines at the bottom of the Fraunhofer lines, denoted by p_{01} and p_{02}.

In this chapter, the method of reducing the experimental data to obtain the plot of ln p_e versus sec.α will be described. The results obtained and a discussion of them will also be presented.

4.2 Method of Analysis

The theory as described in Chapter 3 showed that the abundance of free sodium atoms N in the upper atmosphere could be calculated from the relation

$$\tau_e = \bar{k}N$$

The effective value of the optical thickness τ_e could be obtained from equation (3.30); i.e.,

$$\ln p_{e1} = \ln p_{01} - \tau_{e1} \sec.\alpha \qquad \text{for } D_1\text{-line}$$

and $$\ln p_{e2} = \ln p_{02} - \tau_{e2} \sec.\alpha \qquad \text{for } D_2\text{-line}$$

A plot of $\ln p_e$ versus $\sec.\alpha$ yielded the value of τ_e in the gradient and extrapolation of the graph to $\sec.\alpha = 0$; i.e., no terrestrial absorption by sodium gave the values of p_0, the residual intensities at the bottom of the Fraunhofer lines.

In order to obtain the above-mentioned quantities, the values of p_e and $\sec.\alpha$ must be known, and they could be procured in the way described as follows. During an observation made at a particular time, four spectra as shown in Fig. 2.2 were obtained. The information obtainable from these chart records were: (1) the relative values of d_S, d_L, B_L, and B_S together with the correction for the depth of the Fraunhofer lines--qb_S--which must be added to the measured intensities of the sodium D-lines in spectrum (a) in Fig. 2.2; and (2) the time of observation as indicated by the clock (i.e., Central Standard Time). The chart readings in the quantities observed yielded the values of p_{e1} and p_{e2} for the D_1 and D_2 lines respectively at a particular time of observation. The quantities p_{e1} and p_{e2} were calculated using the following relations:

$$p_{e1} = \frac{D_{S1} \times B_L}{D_{L1} \times B_S}$$

$$p_{e2} = \frac{D_{S2} \times B_L}{D_{L2} \times B_S}$$

where $D_{S1} = d_{S1} + q_1 b_S$ and $D_{S2} = d_{S2} + q_2 b_S$. From these, the values of $\ln p_{e1}$ and $\ln p_{e2}$ as required were obtained.

In order to obtain the quantity sec.α, where α is the angle between the solar ray and the normal to the layer at the point of intersection, the first step was to obtain a functional relationship between sec. α and the angle of elevation of the sun above the horizon, denoted by h. The expression obtained was as follows (Scrimger, 1956):

$$\sec.\alpha = \left[1 - \left(\frac{R \cos. h}{R + H}\right)^2\right]^{-\frac{1}{2}} \quad \ldots (4.1)$$

where R = radius of the earth and H = height of sodium layer. Values of sec. α were obtained for H values of 88 km. and 92 km. in accordance to the sodium layer height obtained by Bullock and Hunten (1961) and plotted against h, which varies from 0 degrees to 60 degrees in steps of 2 degrees. Two curves relating sec. α and h were obtained by this procedure. These curves were very close together, showing that sec. α

values were not critically dependent on the layer height within this region. The observed sec. α values were then deduced through the aid of the time of observation, since the angle of elevation of the sun above the horizon could be found in terms of the Local Apparent Time (L.A.T.) of the particular observation. The time of observation as indicated by the clock (i.e., Central Standard Time) was first converted into Mountain Standard Time (M.S.T.) and the Local Apparent Time was then calculated by means of the following relation:

$$\text{L.A.T.} = \text{M.S.T.} - 6^m30^s + E \qquad \ldots (4.2)$$

where E is the equation of time and -6^m30^s is the correction for the longitude of Saskatoon, 106° 36' W. Knowing the L.A.T. of the particular observation and also the apparent declination of the sun on the particular day during which the run was made, the elevation of the sun h was obtained using the Hunten nomogram. The nomogram, which was designed for Saskatoon (latitude 52° 10'), was used throughout the whole period of observation. The apparent declination of the sun and the equation of time E were obtained from the American Ephemeris and Nautical Almanac, 1963. Having found the value of h for each particular time of observation, the corresponding sec. α value was obtained from the curve of sec. α versus h. This process was carried out for each observation during

a whole run and a series of values of ln p_e and sec. α were thus obtained. Since the relationship between ln p_e and sec. α is linear, a straight line should result. In order to acquire the most probable straight line through all the experimental points, the method of least squares was employed. The process was carried out using a Marchant desk calculator. The least square fit yielded the gradient of the line which was the effective optical thickness required, and extrapolation of the straight line to sec. α = 0 yielded the value of p_O. The probable error in the resultant slope for one run was obtained. The abundance of free sodium atoms N for each D-line was then obtained using the graphs of $\bar{k}N_T$ against N_T in Fig. 3.8a and b.

4.3 Experimental Results

The results presented here were obtained during the months of January, February, March, April, and July, 1963. Plots of ln p_e against sec. α are shown in Figs. 4.1-4.13. As mentioned before, the most probable straight lines through the experimental points were obtained by the method of least squares. The values of the optical thickness τ_e obtained for each D-line and the corresponding sodium abundances are tabulated in Table 4.1. The average sodium abundances are also shown. The residual intensities, p_{O1} and p_{O2} are shown in Table 4.2. The mean value for each D-line is also calculated.

Figs. 4.1-4.13

Plots of ln p_e vs. sec.α, the relative path length of the solar beam. The straight lines were obtained by the method of least squares.

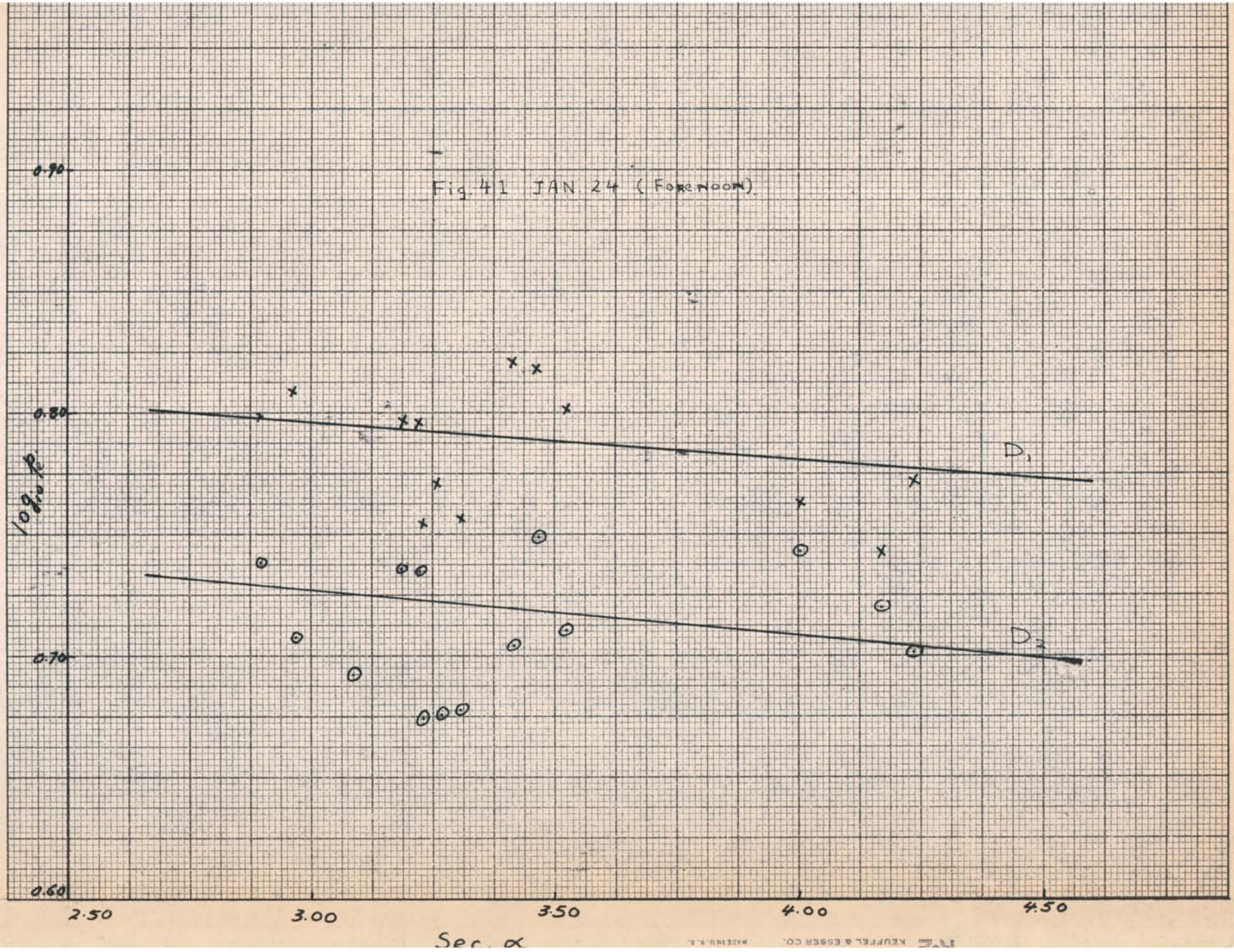
Fig. 41 JAN. 24 (FORENOON)
0.90
0.80
0.70
0.60
$\log_{10} I_2$
D1
D2
2.50
3.00
3.50
4.00
4.50
Sec. α

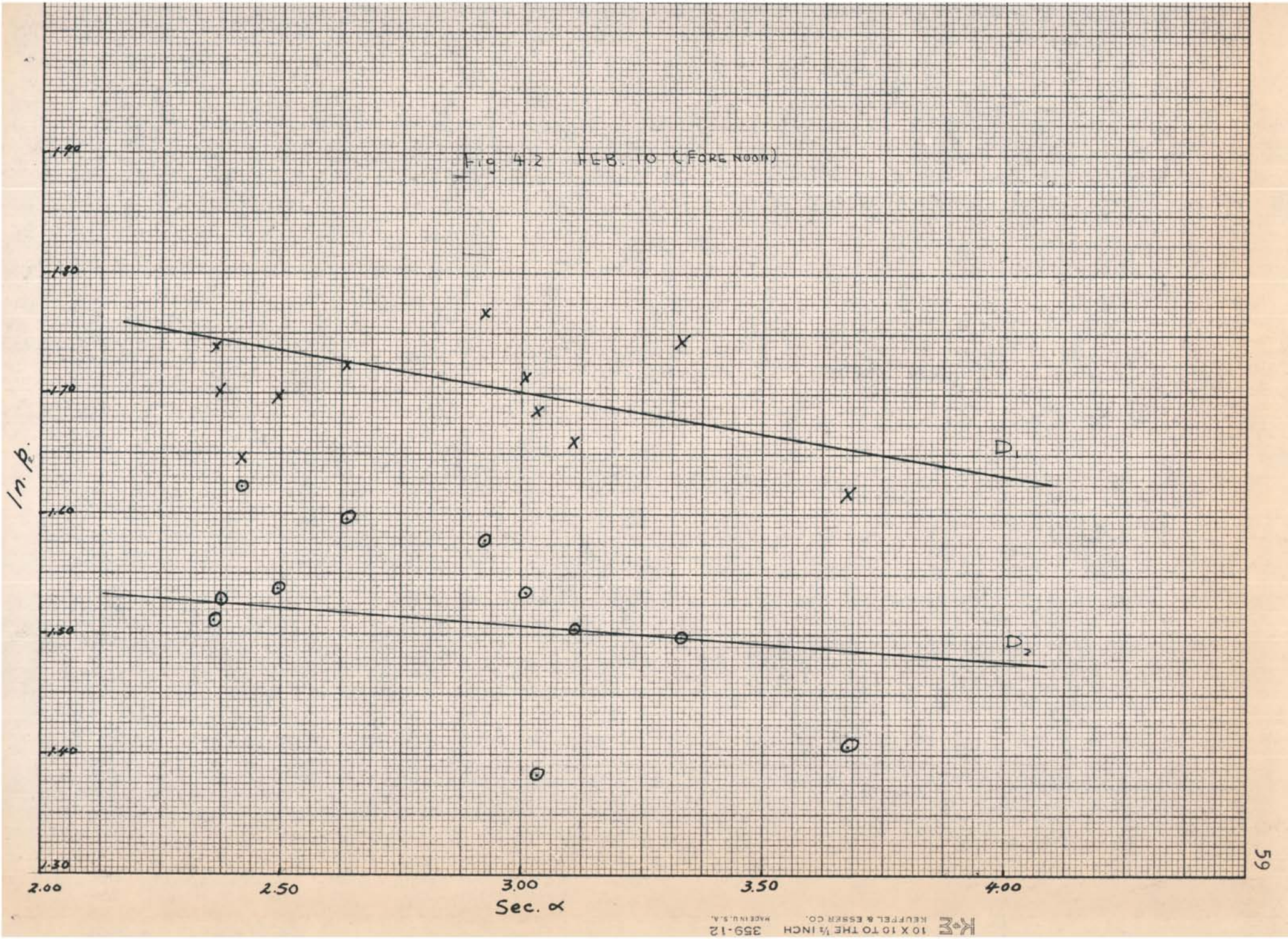
Fig 4.2 FEB. 10 (FORENOON)
1.90
1.80
1.70
1.60
1.50
1.40
1.30
ln. p.
2.00
2.50
3.00
3.50
4.00
Sec. ∝
D1
D2

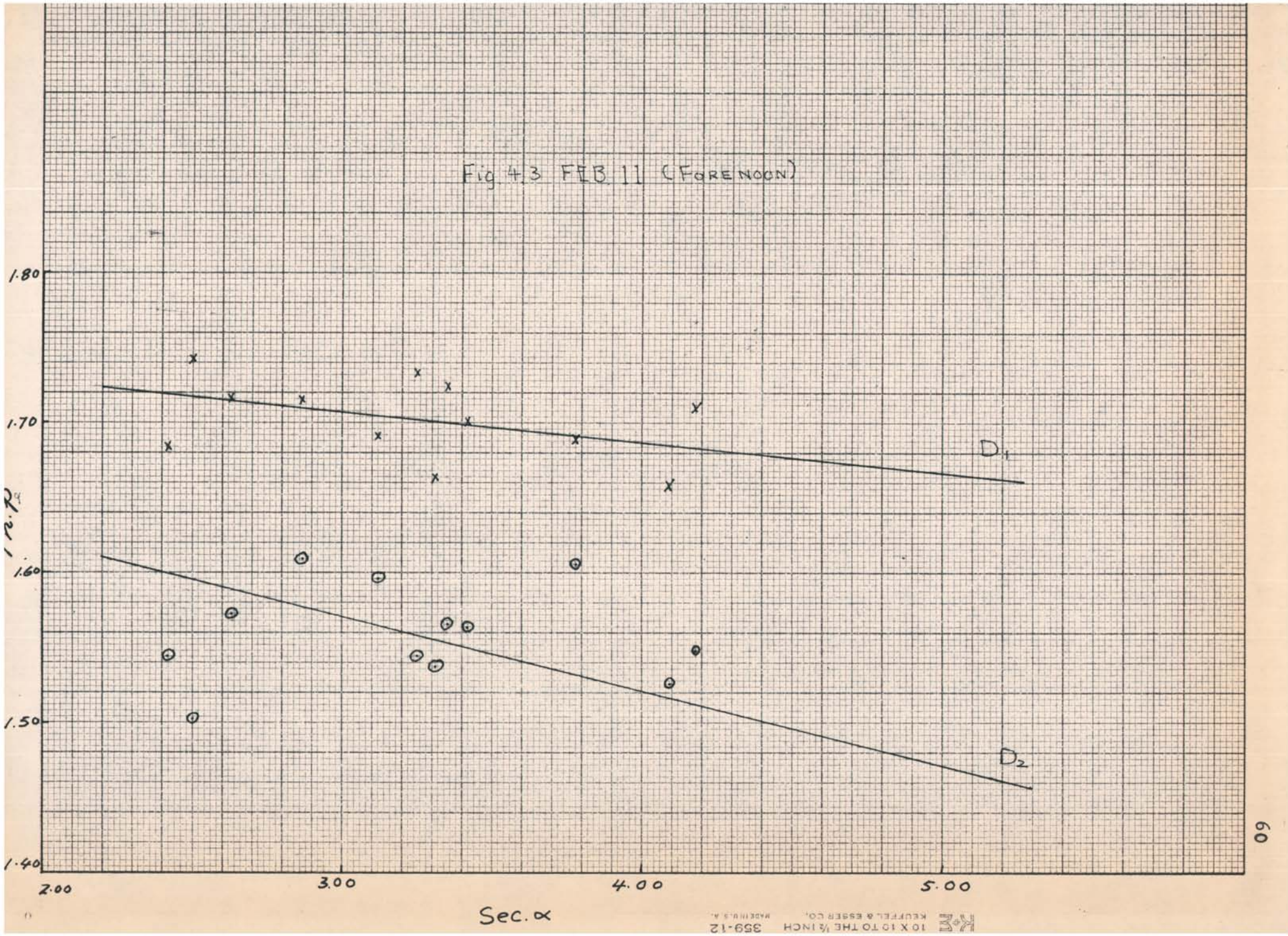
Fig 4.3 FEB 11 (FORENOON)
1.80
1.70
1.60
1.50
1.40
I/I₀.R
D₁
D₂
2.00
3.00
4.00
5.00
Sec. α
KEUFFEL & ESSER CO. MADE IN U.S.A. 359-12
10 X 10 TO THE ½ INCH

Fig. 44 FEB. 19 (AFTERNOON)
D1
D2
ln P
1.80
1.70
1.60
1.50
1.40
1.30
2.00
2.50
3.00
3.50
Sec. x
K&E 10 X 10 TO THE ½ INCH 359-12
KEUFFEL & ESSER CO. MADE IN U.S.A.

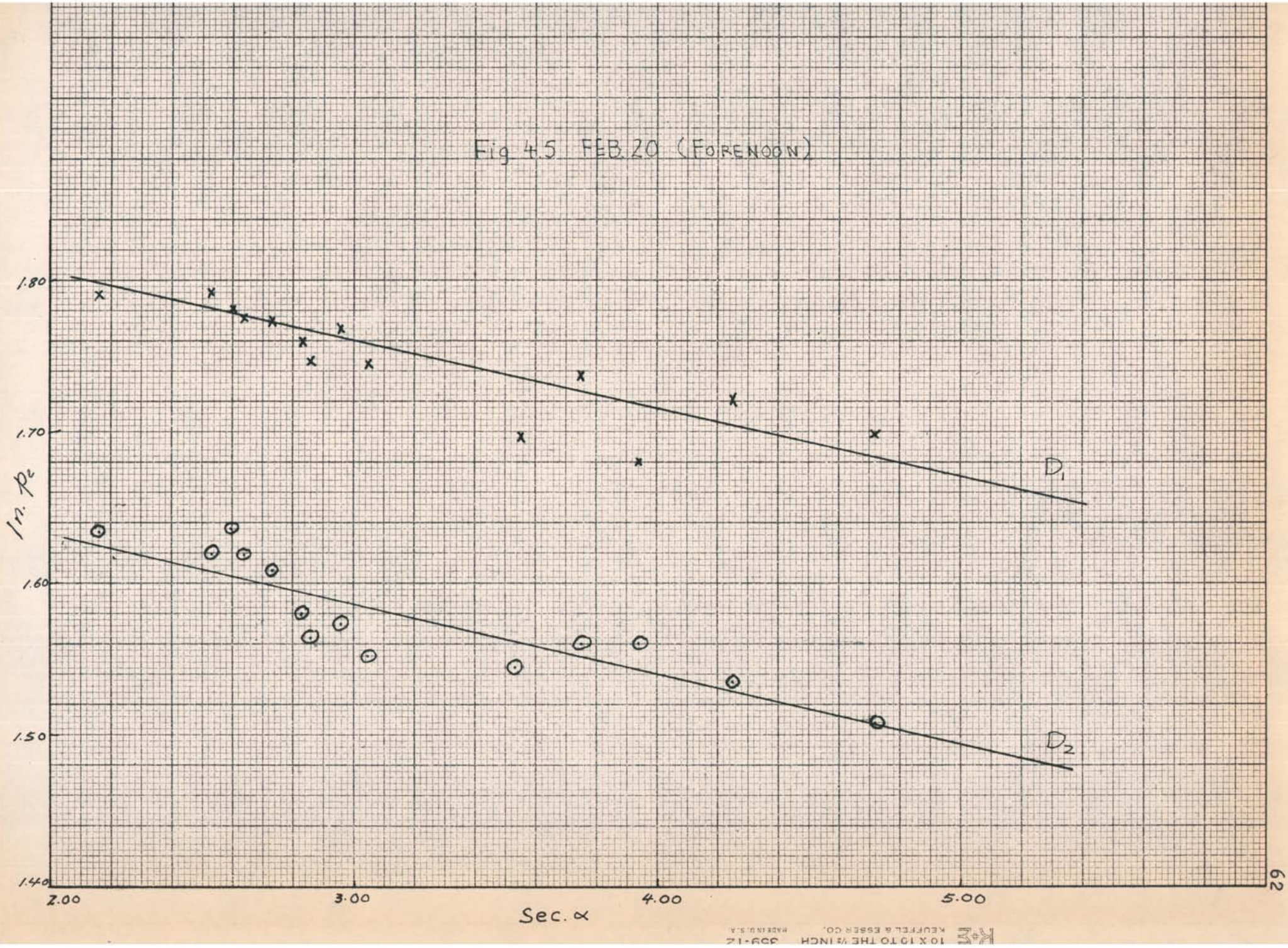
Fig 4.5 FEB. 20 (FORENOON)
1.80
1.70
1.60
1.50
1.40
ln. p2
D1
D2
2.00
3.00
4.00
5.00
Sec. α

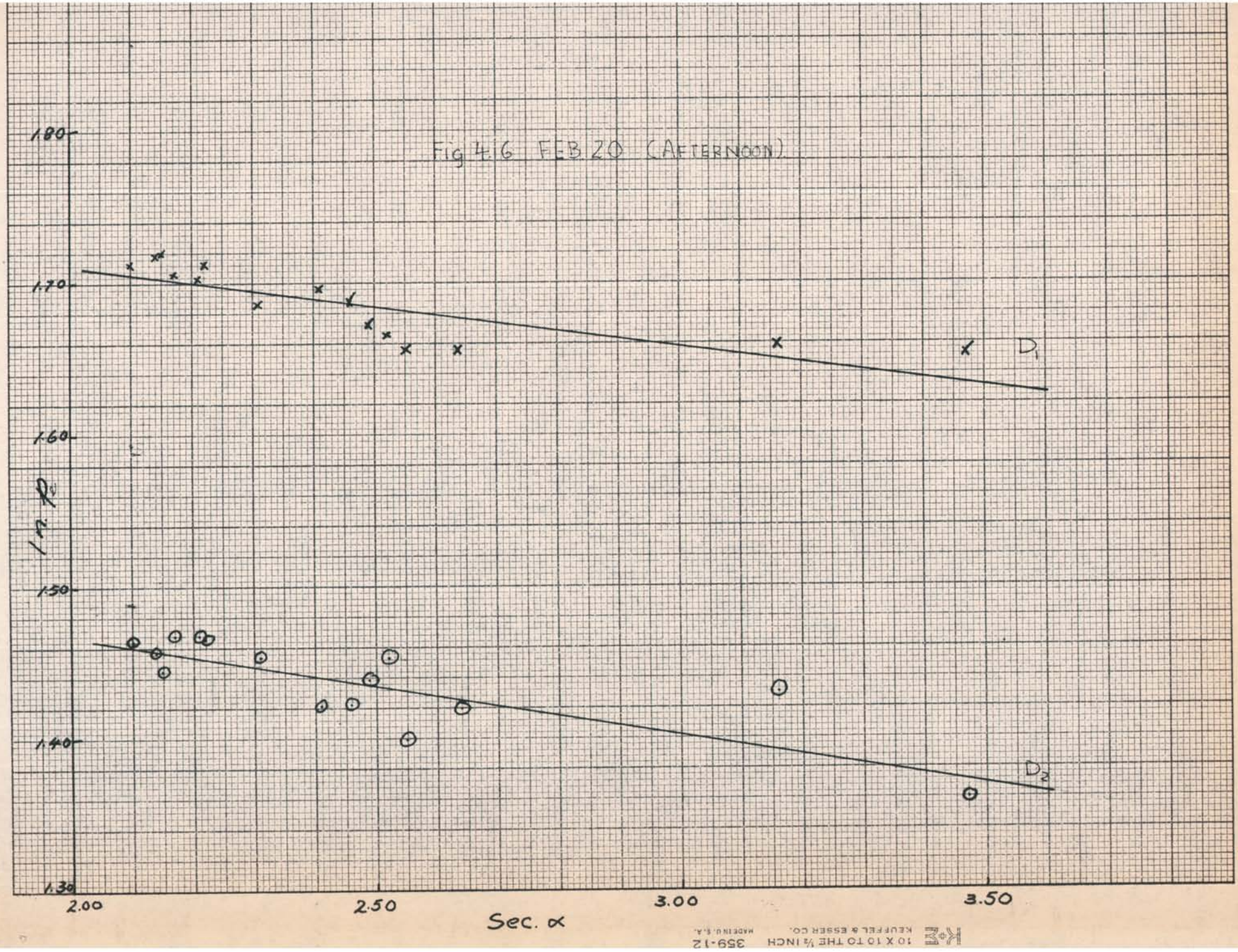
Fig 4.6 FEB 20 (AFTERNOON)
1.80
1.70
1.60
1.50
1.40
1.30
2.00
2.50
3.00
3.50
Sec. α
D1
D2

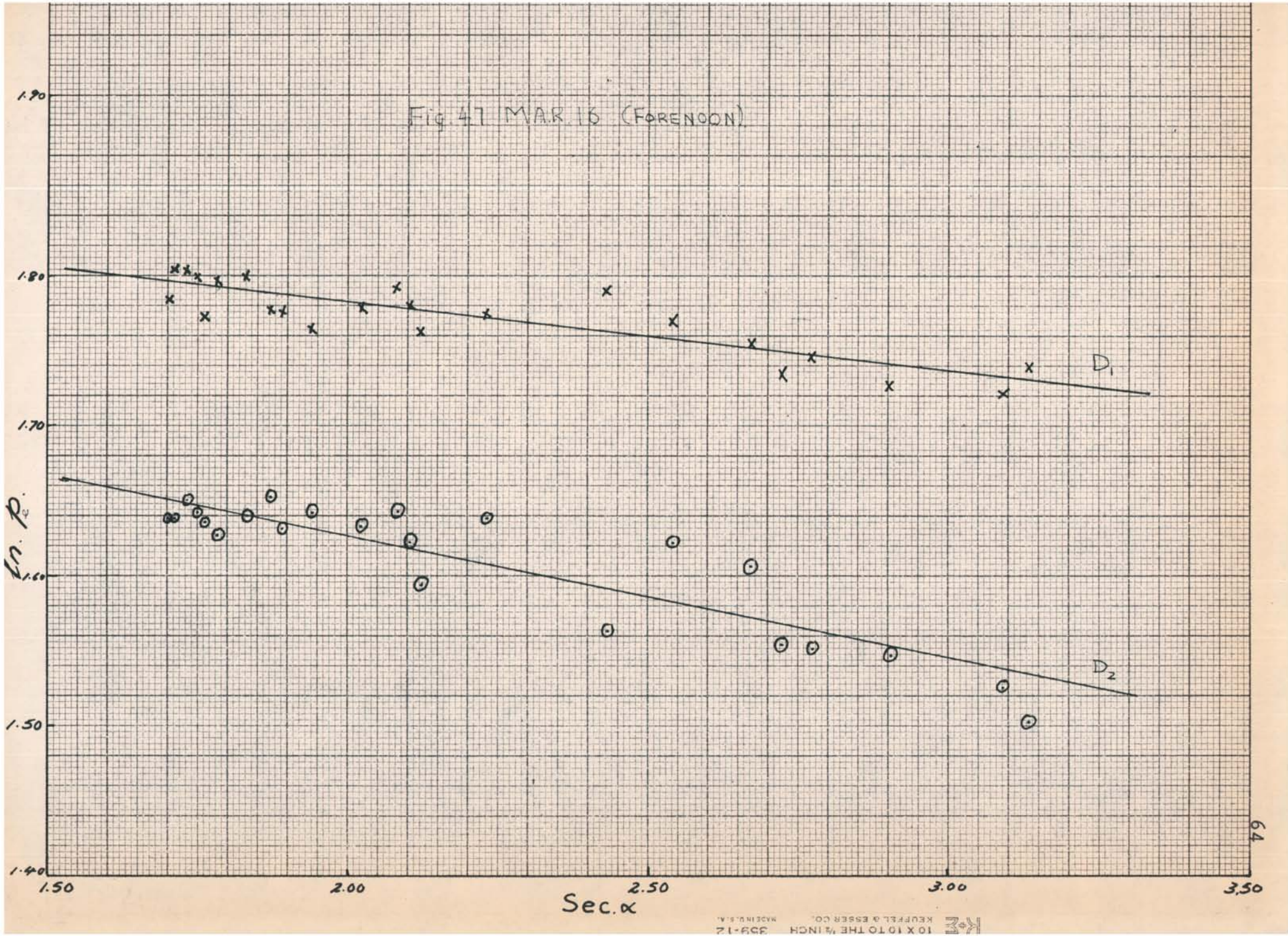
Fig 47 MAR 16 (FORENOON)
1.90
1.80
1.70
1.60
1.50
1.40
Ln. p
1.50
2.00
2.50
3.00
3.50
Sec. α
D1
D2

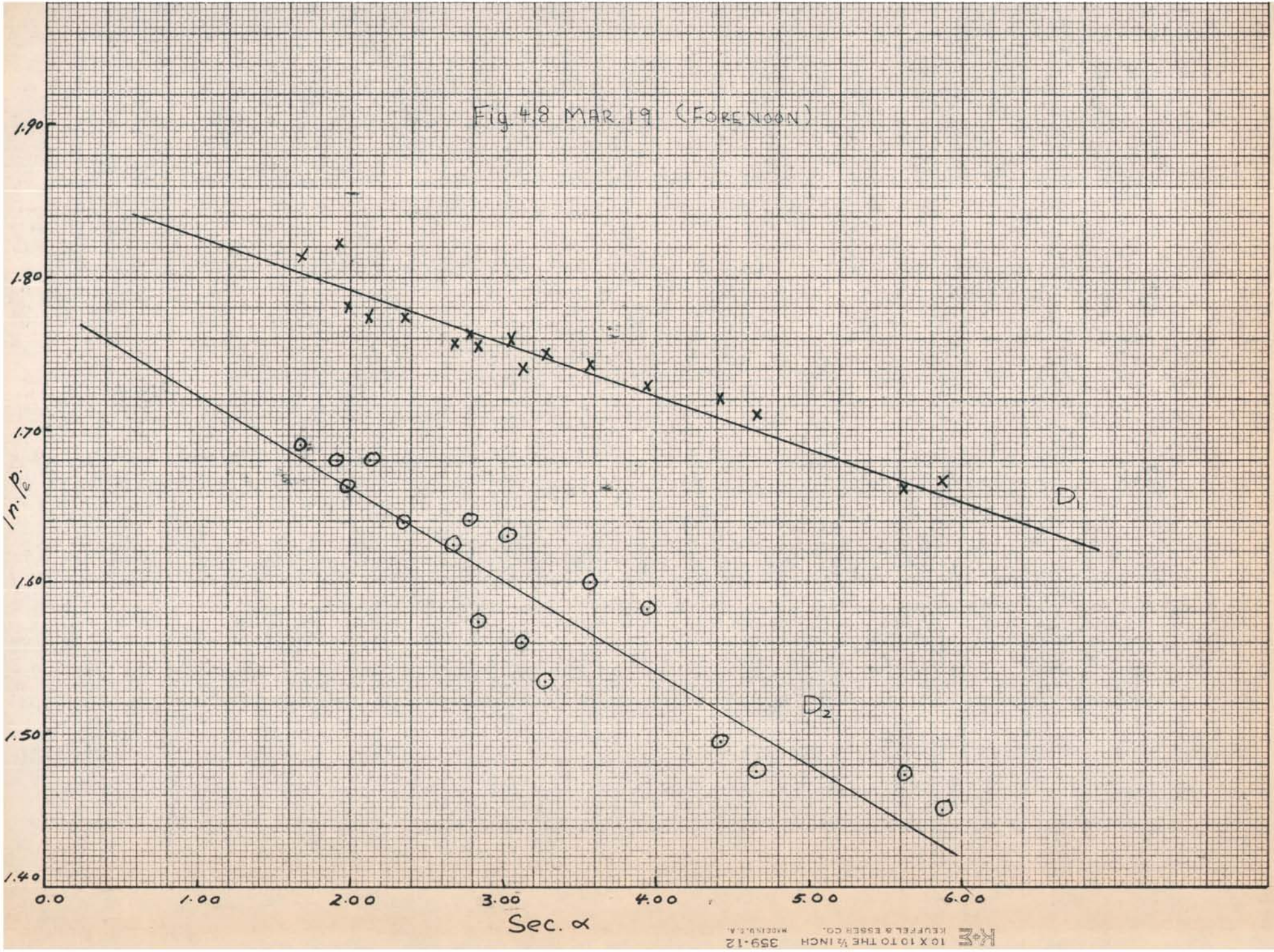
Fig. 4.8 MAR. 19 (FORENOON)
1.90
1.80
1.70
1.60
1.50
1.40
ln. p_2
0.0
1.00
2.00
3.00
4.00
5.00
6.00
Sec. α
D_1
D_2

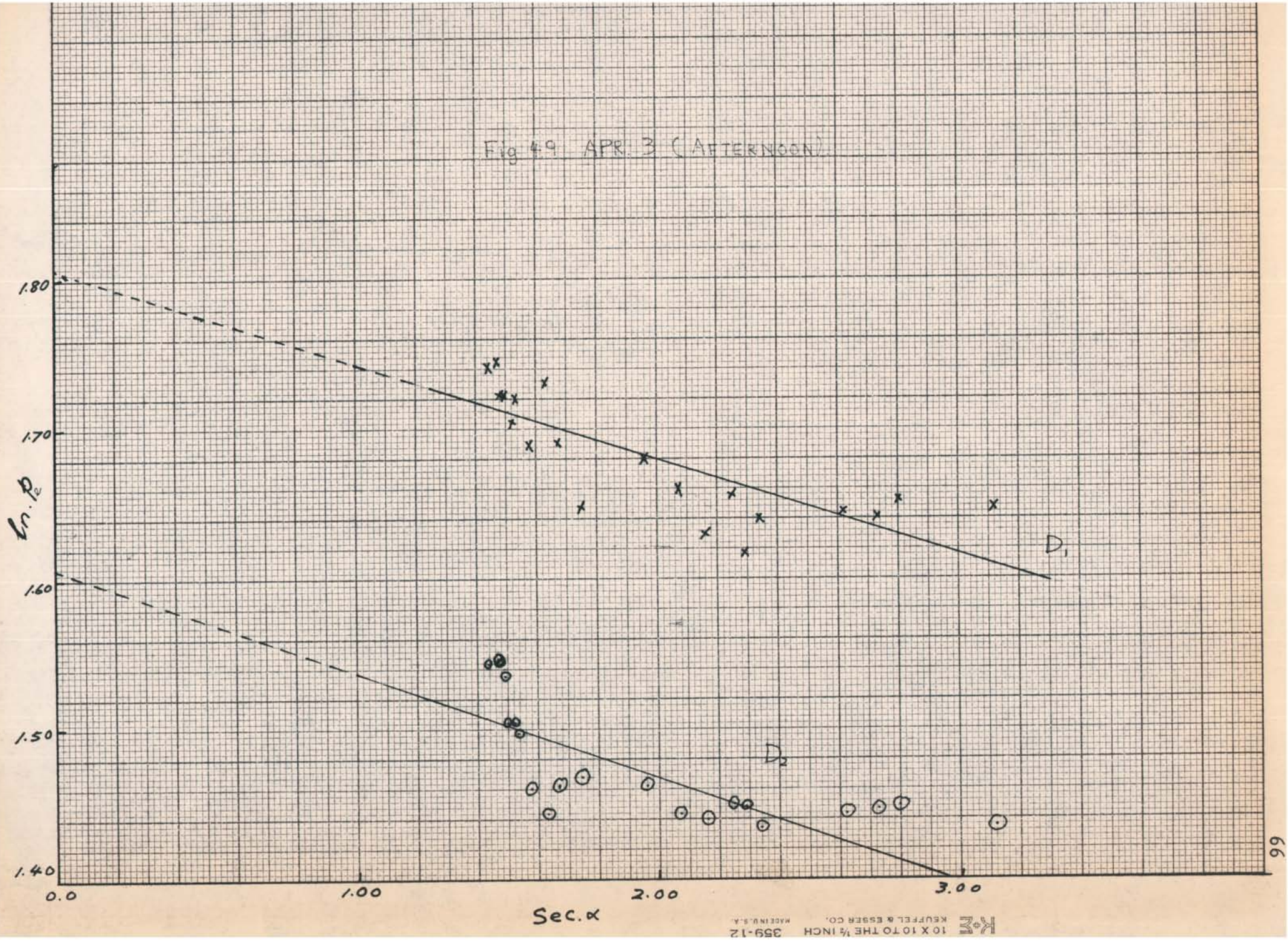
Fig 49 APR. 3 (AFTERNOON)
1.80
1.70
1.60
1.50
1.40
ln. P_2
0.0
1.00
2.00
3.00
Sec. α
D_1
D_2

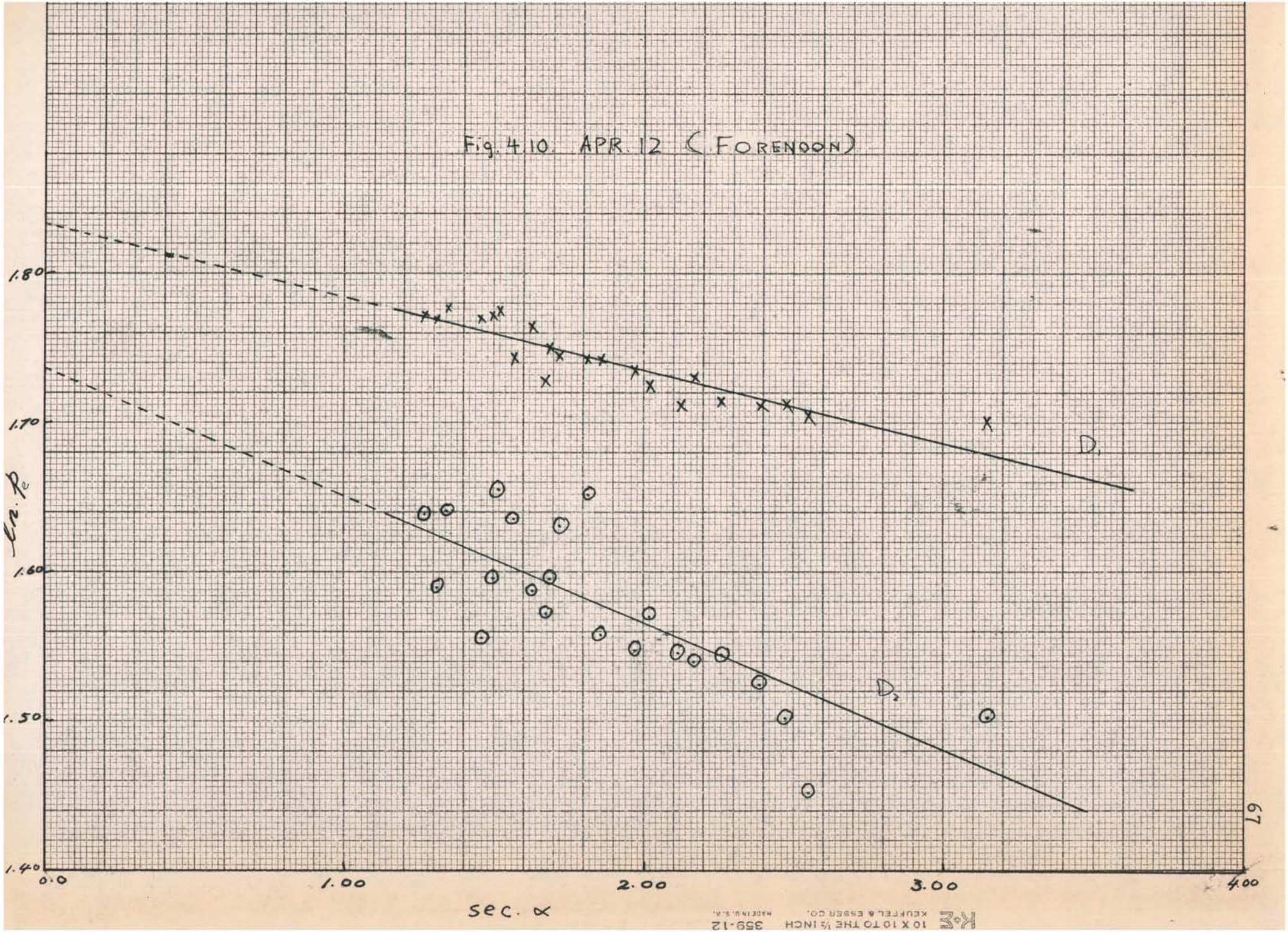
Fig. 4.10. APR. 12 (FORENOON)
1.80
1.70
1.60
1.50
1.40
Ln. Re
0.0
1.00
2.00
3.00
4.00
sec. α
D₁
D₂

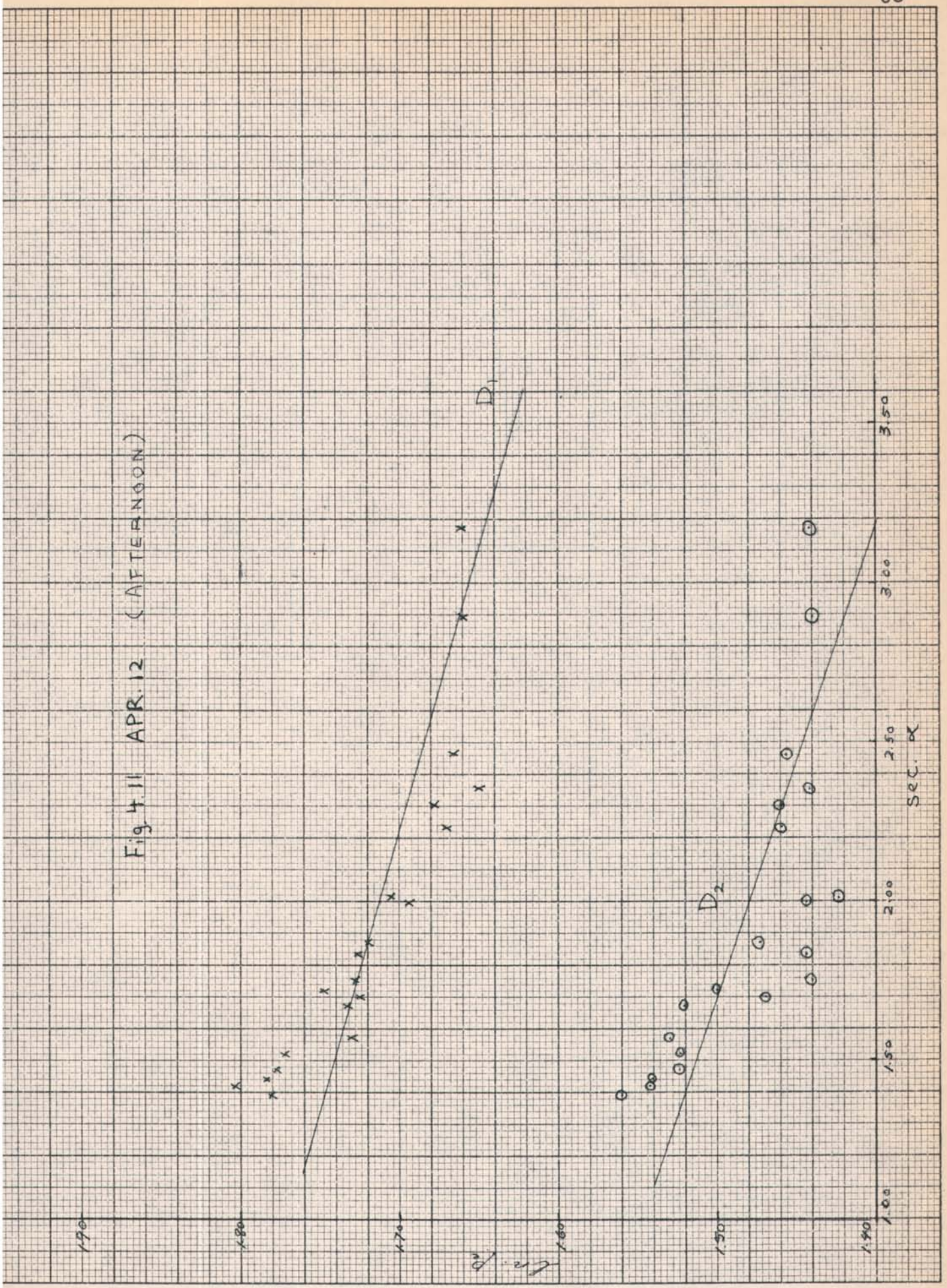

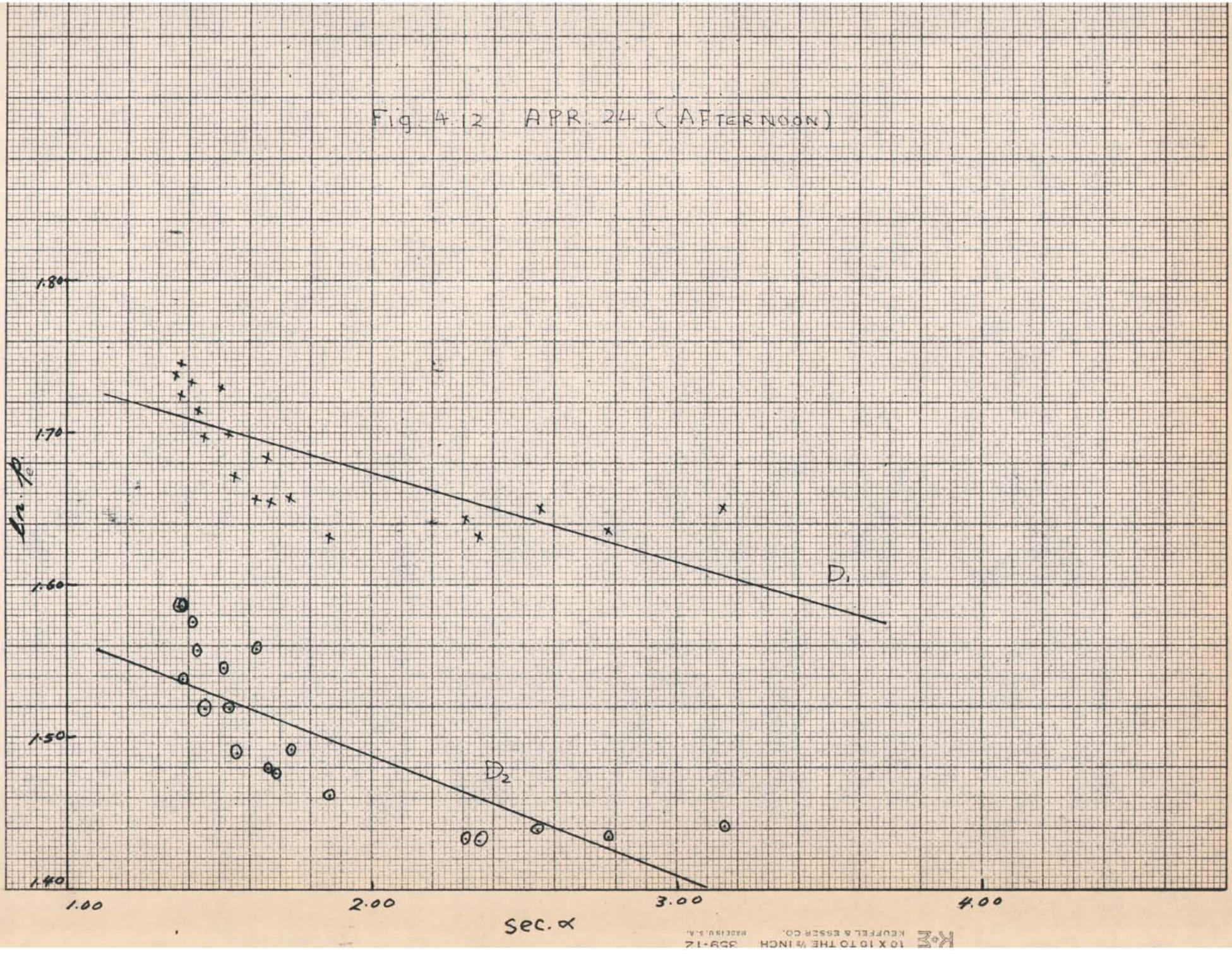
Fig. 4.12 APR. 24 (AFTERNOON)
1.80
1.70
1.60
1.50
1.40
1.00
2.00
3.00
4.00
sec. α
D1
D2

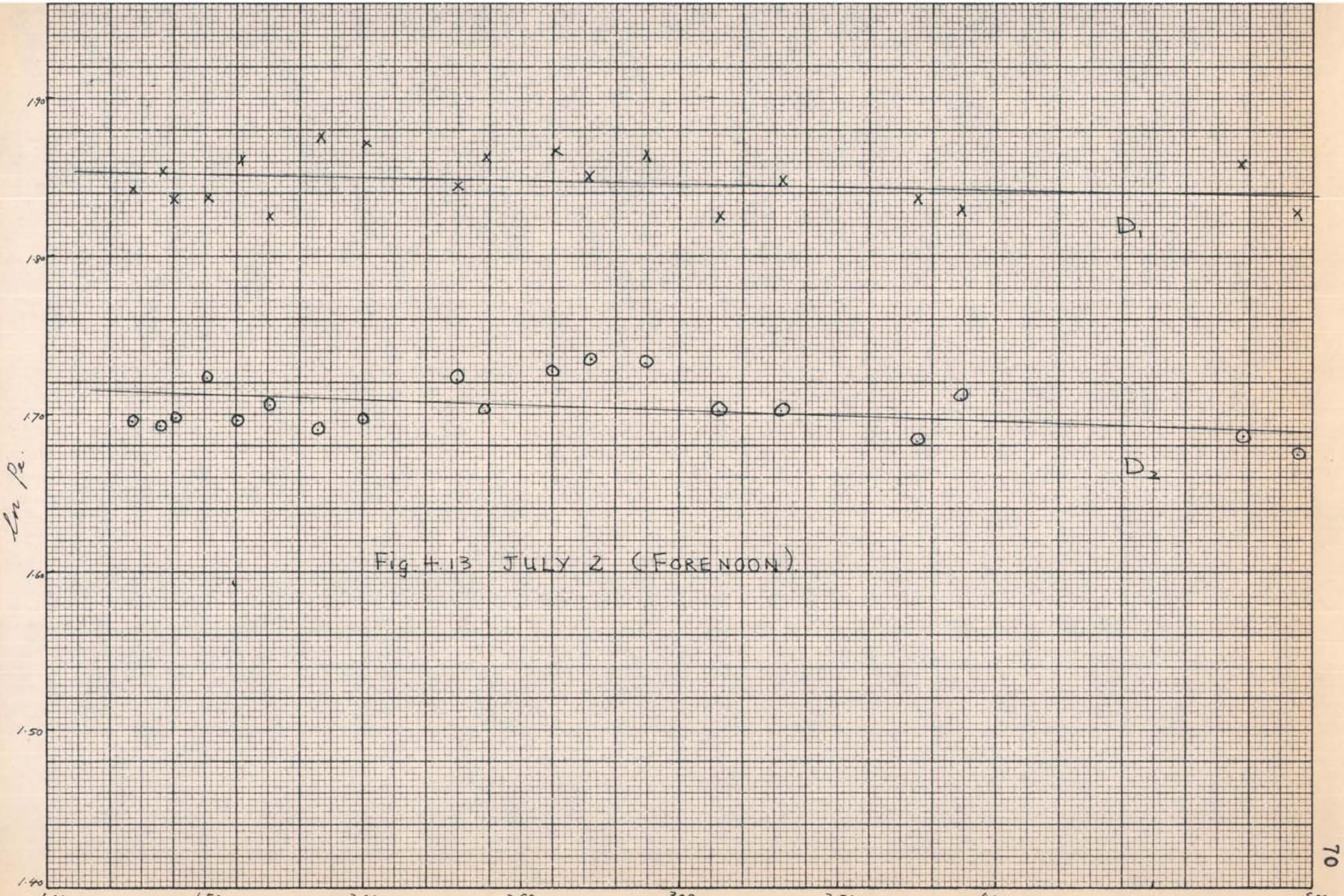

Fig 4.13 JULY 2 (FORENOON)

TABLE 4.1

OBSERVED SODIUM ABUNDANCES

Date	$\tau_e(D_1)$	$\tau_e(D_2)$	Ratio (D_1/D_2)	$N \div 10^9$ (D_1) (atoms/cm^2 column)	$N \div 10^9$ (D_2) (atoms/cm^2 column)	$N \div 10^9$ (average) (atoms/cm^2 column)
Jan. 24 (a.m.)	0.0587	0.0732	0.802	25.5	15.5	20.5
Feb. 10 (a.m.)	0.0349	0.0201	1.736	15.0	4.5	9.8
Feb. 11 (a.m.)	0.0226	0.0503	0.449	9.5	10.5	10.0
Feb. 19 (p.m.)	0.0587	0.0848	0.696	23.0	18.2	20.6
Feb. 20 (a.m.)	0.0465	0.0481	0.967	20.0	10.2	15.1
Feb. 20 (p.m.)	0.0528	0.0622	0.849	22.5	13.2	17.9
Mar. 16 (a.m.)	0.0493	0.0819	0.602	21.3	17.5	19.4

TABLE 4.1--Continued

Date	$\tau_e(D_1)$	$\tau_e(D_2)$	Ratio (D_1/D_2)	$N \div 10^9$ (D_1) (atoms/cm^2 column)	$N \div 10^9$ (D_2) (atoms/cm^2 column)	$N \div 10^9$ (average) (atoms/cm^2 column)
Mar. 19 (a.m.)	0.0342	0.0588	0.582	14.5	11.7	13.1
Apr. 3 (p.m.)	0.0599	0.0647	0.926	26.0	13.8	19.9
Apr. 12 (a.m.)	0.0505	0.0843	0.599	21.7	18.2	20.0
Apr. 12 (p.m.)	0.0537	0.0660	0.815	23.0	14.0	18.5
Apr. 24 (p.m.)	0.0422	0.0824	0.512	18.0	17.5	17.8
July 2 (a.m.)	0.0034*	0.0046**	0.726	1.3	1.1	1.2
Mean			0.789			

*Probable error: ± 0.010

**Probable error: ± 0.011

TABLE 4.2

RESIDUAL INTENSITIES OF THE FRAUNHOFER D-LINES

Date	$p_0(D_1)(\%)$	$p_0(D_2)(\%)$
Jan. 24 (a.m.)	6.97	5.36
Feb. 10 (a.m.)	6.10	4.89
Feb. 11 (a.m.)	5.89	5.42
Feb. 19 (p.m.)	6.45	5.60
Feb. 20 (a.m.)	6.70	5.64
Feb. 20 (p.m.)	6.16	4.92
Mar. 16 (a.m.)	6.59	6.00
Mar. 19 (a.m.)	6.44	5.96
Apr. 3 (p.m.)	6.11	4.92
Apr. 12 (a.m.)	6.29	5.68
Apr. 12 (p.m.)	6.20	5.01
Apr. 24 (p.m.)	6.52	5.20
July 2 (a.m.)	6.42	5.57
Mean	6.37	5.41

4.4 Discussion of Results

The results obtained were presented in Tables 4.1 and 4.2. The effective optical thicknesses τ_e obtained experimentally for both the D_1 and D_2 lines as well as the sodium abundances calculated were shown in Table 4.1. The residual intensities at the bottom of the Fraunhofer D-lines were shown in Table 4.2.

The sodium abundances calculated using the effective absorption coefficient obtained in section 3.3 are unexpectedly high, ranging from 18 X 10^9 to 27 X 10^9 atoms/cm^2 column. A comparison with the sodium abundances obtained by Hunten's photometer on the same day during twilight is shown in Table 4.3. The ratio of daytime to twilight abundance lies in the range of two to six times. On the whole, these results tend to show that the sodium abundance during the day is higher than that during twilight except for one very important factor; i.e., the ratio of the slopes of the optical thicknesses for the D_1 and D_2 lines obtained in the experiment. If the absorption is entirely due to the atmospheric sodium, according to theory, the ratio for $\frac{\tau_e(D_1)}{\tau_e(D_2)}$ or $\frac{\bar{k}(D1)}{\bar{k}(D_2)}$ should be between 0.5 and 0.6. However, the average ratio obtained experimentally was a much higher figure--i.e., 0.79--although there was one run (Feb. 11) which gave a ratio of 0.45. As a result of this discrepancy, it is possible that the results obtained might not give the true sodium

TABLE 4.3

COMPARISON OF SODIUM ABUNDANCES DEDUCED FROM ABSORPTION MEASUREMENTS WITH THOSE OF TWILIGHT

Date	Absorption Measurements (atoms/cm^2 column)	Twilight (atoms/cm^2 column)	Ratio (Day/Twilight
Feb. 10 (a.m.)	99.8×10^9	6.0×10^9	1.6
Feb. 11 (a.m.)	10.0×10^9	4.6×10^9	2.2
Feb. 20 (a.m.)	15.1×10^9	3.2×10^9	4.7
Mar. 16 (a.m.)	19.4×10^9	4.3×10^9	4.5
July 2 (a.m.)	1.20×10^9	$1.3 \times 10^{9*}$	0.9

*Taken from Chamberlain, Hunten, and Mack (1958a).

abundances. Another factor which might contribute to the high sodium abundances obtained involved the calculation of the effective absorption coefficient $\bar{k}$. The values of $\bar{k}$ obtained for low abundances were very small, thus leading to high values of the abundances. It is possible that the assumptions used in deriving $\bar{k}$ may not be valid, especially at low abundances where the calculations become most critical.

High observed $\bar{k}$ values could be absorption by some other constituents, water vapour, for example.

Although the results of the present experiment seemed to indicate higher sodium abundances in the daytime in accordance with what Blamont and Donahue (1961) obtained, work by Zwick and Shepherd (1961) and McNutt and Mack (1963) showed lack of sodium enhancement during the daytime. Zwick and Shepherd (1961) measured the ratio and absolute brightness of the sodium D-lines in the twilight using a low-resolution Fabry-Perot spectrometer, while McNutt and Mack (1963) observed terrestrial absorption of solar radiation by employing a high-resolution Fabry-Perot spectrometer coupled to a grating spectrometer. This discrepancy is yet to be resolved, and one way would be to measure the sodium emission directly. This is at the moment being done by using a high-resolution spectrometer.

The residual intensities at the bottom of the

Fraunhofer D-lines obtained by this experiment and those obtained by other workers are shown in Table 4.4. The results seemed to agree with those of Scrimger and Hunten (1957), the values being 6.37 $\pm$ 0.19% and 5.41 $\pm$ 0.25% for the D_1 and D_2 lines respectively.

TABLE 4.4

COMPARISON OF THE RESIDUAL INTENSITIES (% OF CONTINUUM) WITH THOSE OBTAINED BY OTHER WORKERS

D_1	D_2	D_2/D_1	Region*	References
5.0 ± 0.6	4.8 ± 0.6	0.96	c	Scrimger and Hunten, 1955
5.90 ± 0.46	5.06 ± 0.24	0.86	i	Scrimger and Hunten, 1957
6.6	5.8	0.88	i	Blamont et al., 1958
7.9	6.6	0.84	i	Donahue and Stull, 1959
5.0	4.4	0.88	c	Waddell, 1962
4.95 ± 0.10	4.44 ± 0.10	0.897	i	McNutt and Mack, 1963
6.37 ± 0.19	5.41 ± 0.25	0.85	i	Present work

*i = whole disc, integrated
c = centre of disc

5. SUMMARY AND CONCLUSIONS

The present work is essentially a repeat of the experiment of Scrimger and Hunten (1957). It was prompted by the recent work of Blamont and Donahue (1961), whose results indicated the abundance of sodium in the upper atmosphere to be three to four times more than that measured during twilight. Consequently, the present work was pursued with the purpose of obtaining more evidence regarding the daytime abundance of sodium. The main aim was to observe the variation of absorption by atmospheric sodium as the solar beam passed through the sodium layer, and from this to deduce the sodium abundance. Since the radiation measured was at the bottom of the Fraunhofer D-lines, the residual intensities there were measured as a by-product. A low-resolution Fabry-Perot spectrometer coupled to a sodium vapour cell was employed in the observation. An interference filter of passband half-width 15 Å was used as a monochromator to isolate a single passband. The spectrometer was made to scan through a spectral range of 20 Å once every 50 seconds with 10 seconds recycle. The sodium vapour cell was maintained at

the temperature of 145°-150° C. The observations were performed by using two separate channels--the monitor and the sodium cell channels. Each measurement took two minutes, producing four spectra, two in each channel. A typical run varied from three to five hours in the morning or afternoon.

Altogether, thirteen runs were taken on eleven different days during the period between January and July. The effective optical thicknesses, τ_e, obtained in this experiment are not much different from those obtained by Scrimger and Hunten (1957). However, the method of obtaining the effective absorption coefficient $\bar{k}$ is entirely different. In consequence, the average sodium abundances calculated using the values of $\bar{k}$ obtained are much higher, ranging from 18 X 10^9 to 27 X 10^9 atoms/cm^2 column. A comparison with the results obtained in twilight on the same day showed the daytime sodium abundance to be two to five times more. This tends to support the recent results obtained by Blamont and Donahue (1961). However, two factors tend to make the results obtained a little uncertain. Firstly, the theory indicated that the ratio of the effective optical thicknesses for the D_1 and D_2 lines--i.e., $\frac{\tau_e(D_1)}{\tau_e(D_2)}$ or $\frac{\bar{k}(D_1)}{\bar{k}(D_2)}$ -- was in the range 0.5 to 0.6 while the measured ratio was on the average 0.79. This discrepancy might possibly lead to wrong sodium abundances calculated. Secondly, there exists considerable

doubt regarding the effective absorption coefficient $\bar{k}$. The values of $\bar{k}$ used in calculating the abundances were obtained using the temperature profiles of sodium D-lines during twilight as calculated by Chamberlain, Hunten, and Mack (1958a). The effective absorption coefficients obtained indicated that they increased with increasing abundances. The results might be different if the temperature profiles of the atmospheric sodium during daytime and twilight are different. Thirdly, the run obtained during summer showed disagreement with that obtained by Blamont and Donahue.

The residual intensities at the bottom of the Fraunhofer D-lines obtained were $6.37 \pm 0.19\%$ and $5.41 \pm 0.25\%$. The results seemed to agree with those of Scrimger and Hunten (1957) quite well except that they are slightly higher.

All in all, the present results tend to support the fact that daytime sodium abundance is higher than that obtained during twilight. However, McNutt and Mack (1963) measured the terrestrial absorption of solar radiation using a high resolution Fabry-Perot spectrometer coupled to a grating spectrometer and showed that the daytime abundance of sodium was the same as that during twilight. Work by Zwick and Shepherd (1961) in measuring the ratio and absolute brightness of the sodium D-lines in twilight also indicated no enhancement of sodium during the daytime. The probable way to resolve this discrepancy would be to measure directly

the sodium emission in the daytime. This is being done here by using a high-resolution Fabry-Perot spectrometer. Another way would be to improve the sensitivity of the present instrument, which used only about one-third of the Fabry-Perot etalon. By using a larger coelostat and sodium cell, sensitivity would be greatly improved because the whole etalon could be used. The present instrumental arrangement could be extended by arranging a magnetic field similar to that used by Blamont and Donahue (1961) around the sodium vapour cell. The magnetic field would then shift the passband into the continuum, and the D-line intensity could be obtained by noting the difference between field-on and field-off readings. This method would also allow an abundance to be obtained at a fixed solar elevation, and this could be compared with the variation of solar elevation method. It would also provide a check on the calculations of $\bar{k}$. It could be arranged that the twilight results also be measured by the same instrument. A comparison of these results would probably resolve the discrepancy between the daytime and twilight sodium abundances. This problem is at the moment being seriously considered.

- - -

LIST OF REFERENCES

Allen, C. W., 1939, M.N.R.A.S. 100, 10.

"The American Ephemeris and Nautical Almanac," 1963.

Blamont, J. E. and Donahue, T. M., 1958, Compt. rend. 247, 496.

_____, 1961, J. Geophys. Res. 66, 1407.

Bricard, J. and Kastler, A., 1944, Ann. Geophys. 1, 53.

Brandt, J. C. and Chamberlain, J. W., 1958, J. Atmos. Terr. Phys. 13, 90.

Bullock, W. R. and Hunten, D. M., 1961, Can. J. Phys. 39.

Chabbal, R., 1953, J. recherches centre natl. recherche sci. 24, 138.

_____, 1958a, Theses Universite de Paris.

_____, 1958b, J. Phys. radium, 19, 246.

Chamberlain, J. W., Hunten, D. M., and Mack, J. E., 1958a, J. Atmos. Terr. Phys. 12, 153-165.

Chamberlain, J. W., 1961, "Physics of the Aurora and Airglow" (Academic Press, New York & London).

Cogger, L. L., 1962, M.A. Thesis, University of Saskatchewan.

Donahue, T. M. and Stull, V. R., 1959, Ann. Geophys. 15.

Donahue, T. M., 1956a, J. Geophys. Res. 61, 663-666.

Hunten, D. M., A monogram for solving spherical triangles. Scientific Report No. BR. 8, Phys. Dept., University of Saskatchewan, Saskatoon, Sask., Canada.

Jacquinot, P., 1954, J. Opt. Soc. Am. 44, 761.

_____, 1960, Rep. Prog. Phys. 23, 267.

McNutt, D. P., 1962, Ph.D. Thesis, University of Wisconsin.

McNutt, D. P. and Mack, J. E., 1963, J. Geophys. Res. 11, 3419-3429.

Nilson, J. A., 1960, M.Sc. Thesis, University of Saskatchewan.

Nilson, J. A. and Shepherd, G. G., 1961, Planet. Sp. Sci. 5, 299.

Priester, W., 1933, Z. Astrophys. 32.

Scrimger, J. A., 1954, M.Sc. Thesis, University of Saskatchewan.

_____, 1956, Ph.D. Thesis, University of Saskatchewan.

_____ and Hunten, D. M., 1957, Can. J. Phys. 35, 918-927.

Shane, 1941, Lick Obs. Bull. No. 507, Table 2, p. 123.

Shepherd, G. G., 1960, Can. J. Phys. 38.

Turgeon, E. C. and Shepherd, G. G., 1962, Planet. Sp. Sci. 9, 295.

Waddell, J., 1962, Astrophys. J. 136.

Zwick, H. H., 1962, M.Sc. Thesis, University of Saskatchewan.

Zwick, H. H. and Shepherd, G. G., 1963, Can. J. Phys. 41.

- - -